

Semileptonic $D \rightarrow V(\omega, \rho, K^*)\ell^+\nu_\ell$ decays within QCD light-cone sum rule approach

Hai-Bing Fu¹ , Wei Cheng^{†,2} , Long Zeng¹ and Dan-Dan Hu¹

¹*Institute of Particle Physics & Department of Physics, Guizhou Minzu University, Guiyang 550025, P.R. China*

²*State Key Laboratory of Theoretical Physics, Institute of Theoretical Physics, Chinese Academy of Sciences, Beijing, 100190, P.R. China*

[†]Corresponding author

E-mail: chengwei@itp.ac.cn

ABSTRACT: In the paper, the physical observables for $D \rightarrow V(\omega, \rho, K^*)\ell^+\nu_\ell$ semileptonic decays are investigated thoroughly with the SSE extrapolated HFFs, which are calculated within the framework of QCD LCSR and up to twist-4. For the decay width parts, we find that $1/|V_{cq}|^2 \times \Gamma^{\text{L,T,total}}(D \rightarrow V\ell^+\nu_\ell)$ decrease with the increase of final meson mass, and the absolute change number of the transverse and longitudinal are almost the same. The transverse differential decay width dominates in the small q^2 region, while the longitudinal differential decay width dominates in the large q^2 region, and the dominant alternate point is near the midpoint of the whole physically feasible region. We then calculate the branching fractions by applying the $D^0(D^+)$ meson lifetime from the Particle Data Group, i.e. $\mathcal{B}(D^0 \rightarrow \rho^- e^+ \nu_e, \rho^- \mu^+ \nu_\mu) = (1.440^{+0.277}_{-0.250}, 1.432^{+0.274}_{-0.248}) \times 10^{-3}$ and $\mathcal{B}(D^+ \rightarrow \rho^0 e^+ \nu_e, \rho^0 \mu^+ \nu_\mu) = (1.827^{+0.351}_{-0.317}, 1.816^{+0.348}_{-0.314}) \times 10^{-3}$ for ρ meson channel; $\mathcal{B}(D^+ \rightarrow \omega^0 e^+ \nu_e, \omega^0 \mu^+ \nu_\mu) = (1.740^{+0.482}_{-0.399}, 1.728^{+0.479}_{-0.397}) \times 10^{-3}$ for ω meson channel; $\mathcal{B}(D^0 \rightarrow K^{*-} e^+ \nu_e, K^{*-} \mu^+ \nu_\mu) = (2.082^{+0.334}_{-0.314}, 2.066^{+0.330}_{-0.310}) \times 10^{-2}$ and $\mathcal{B}(D^+ \rightarrow \bar{K}^{*0} e^+ \nu_e, \bar{K}^{*0} \mu^+ \nu_\mu) = (5.282^{+0.847}_{-0.796}, 5.242^{+0.838}_{-0.787}) \times 10^{-2}$ for K^* meson channel. All those branching fraction results are lower compared to other theories, but fits well with BES-III predictions within errors. For the polarization parts, we study in detail the q^2 dependence of longitudinal and transverse polarizations fractions of the charged lepton and the vector meson in the final state, i.e. $P_{\text{L,T}}^\ell$ and $F_{\text{L,T}}^\ell$, the forward-backward asymmetry $\mathcal{A}_{\text{FB}}^\ell$ and the lepton-side convexity parameters \mathcal{C}_ℓ . In the small q^2 region, all those polarization observations have a singularity due to the δ_ℓ factor, except for $F_{\text{L,T}}^\ell$. With the increase of q^2 , all polarization values tend to be more stable, thus the polarization dependence on q^2 is smaller. Our predictions for their corresponding average values have agreement with the theoretical group for Covariant Confining Quark Model results within the errors.

Contents

1	Introduction	1
2	Calculation Technology	3
2.1	$D \rightarrow V \ell^+ \nu_\ell$ semileptonic decays	3
2.2	$D \rightarrow V$ HFFs	6
3	Numerical Analysis	9
3.1	LCDAs and $D \rightarrow V$ HFFs	9
3.2	D Meson Semileptonic Decays	12
3.2.1	Decay width	12
3.2.2	Polarization observations	15
4	Summary	20

1 Introduction

Semileptonic $D \rightarrow V \ell^+ \nu_\ell$ decays are the significant component for a comprehensive understanding of the particle standard model (SM) in the post-Higgs era. Those decays not only are directly related to CKM matrix elements, which provide a window to research CP-violation problem of the SM [1–8], but also contain the flavour-changing neutral current (FCNC) processes, which are sensitive to new physics (NP) due to it occurs at least one loop level in SM [9–13].

Normally, the semileptonic $D \rightarrow V(\omega, \rho, K^*) \ell^+ \nu_\ell$ decays can be embodied as three different sets of form factors in terms of underlying quark transitions, which are listed in Table 1. For study those decays, decay width and branching fraction are the first important observations, which have been studied by BES-III [14–20] and CLEO [21–26] collaboration extensively. For example, in 2019, BES-III collaboration measure the $D \rightarrow \rho \ell \nu_\ell$ branching fraction, i.e. $\mathcal{B}(D^0 \rightarrow \rho^- e^+ \nu_e) = (1.445 \pm 0.058_{\text{stat}} \pm 0.039_{\text{syst}}) \times 10^{-3}$ and $\mathcal{B}(D^+ \rightarrow \rho^0 e^+ \nu_e) = (1.860 \pm 0.070_{\text{stat}} \pm 0.061_{\text{syst}}) \times 10^{-3}$ [17], meanwhile they also present an improved measurement for the $D \rightarrow K^*(892)^- e^+ \nu_e$ branching fraction, i.e. $\mathcal{B}(D^0 \rightarrow K^*(892)^- e^+ \nu_e) = (2.033 \pm 0.046_{\text{stat}} \pm 0.047_{\text{syst}}) \times 10^{-2}$ [18] in the same year. It is worth noting that BES-III recently published their first measurements for the $D^+ \rightarrow \omega \mu^+ \nu_\mu$ branching fraction in the year 2020, i.e. $\mathcal{B}(D^+ \rightarrow \omega \mu^+ \nu_\mu) = (17.7 \pm 1.8_{\text{stat}} \pm 1.1_{\text{syst}}) \times 10^{-4}$, which is realized by applying an $e^+ e^-$ collision data sample corresponding to an integrated luminosity of 2.93 fb^{-1} collected with the BESIII detector at a center-of-mass energy of 3.773 GeV [27].

Table 1. Allowed $D \rightarrow V$ decay channels in terms of underlying quark transitions.

	ρ^0, ω	ρ^-	K^{*-}	$\bar{K}^{*0}(s\bar{d})$
D_u^0	—	$c \rightarrow d$	$c \rightarrow s$	—
D_d^+	$c \rightarrow d$	—	—	$c \rightarrow s$

To further systematic understanding of the $D \rightarrow V$ semileptonic, one may need to know the full angular distribution and polarization information, such as the longitudinal and transverse polarizations of the final charged lepton $P_{\text{L,T}}^\ell(q^2)$ and the final vector meson $F_{\text{L,T}}^\ell(q^2)$, the forward-backward asymmetry $\mathcal{A}_{\text{FB}}^\ell(q^2)$, and the lepton-side convexity parameter $\mathcal{C}_F^\ell(q^2)$. But there are few theoretical research for those polarization information and even fewer experimental ones. Consider the numerous experimental and theoretical studies for that of the B -meson [28–37], we will study those observations for the semileptonic $D \rightarrow V\ell^+\nu_\ell$ decays within the framework of QCD light-cone sum rules (LCSR).

The LCSR is one of important method for dealing with the meson semileptonic decays [38–47]. Its main strategy is to construct an analytic heavy-to-light correlator function in the whole q^2 region and then make an operator product expansion (OPE) and a hadron expression for it in the spacelike and timelike region respectively, finally combine two expressions with the help of Borel transformation to get the TFFs or HFFs. Both of TFFs and HFFs contain the information for meson semileptonic decays independently, the reason is that they can describe the non-perturbative hadronic matrix elements of meson semileptonic decays independently. One can decompose the hadronic matrix elements by applying momentum of initial and final meson states to obtain TFFs [48–54], which will lead to a mixing of longitudinal and transverse polarization of the meson among those TFFs. Thus TFFs cannot express the polarization information of meson decay accurately.

The HFFs opened new avenues to deal with those matrix elements [55–57]. HFFs decompose it by applying the off-shell W -boson polarization vectors, which imply good polarization properties, enabling polarization tracking studies. Specifically, the longitudinal and transverse decay information can be completely separated, which is very useful for probing the longitudinal and transverse polarization separately. For example, both of the decay width of D -meson longitudinal and transverse components contain the usual TFF ($A_1(q^2)$), which means D -meson longitudinal and transverse components are interplays. While, in HFFs cases, the decay widths of D -meson longitudinal (transverse) component refer to $\mathcal{D}_{V,0}(q^2)$ ($\mathcal{D}_{V,1}(q^2)$, $\mathcal{D}_{V,2}(q^2)$) HFF. In addition to the above advantages, it also has some other advantages, e.g. dispersive bounds on the HFF parametrization and direct relations between the HFFs and the spin-parity quantum numbers, which are listed in Table 2. More detail discussion can refer to the literature [55–57].

The rest of the paper is organized as follows. In Section 2, we introduce the physical ob-

Table 2. Resonance masses of quantum number J^P as indicated necessary for the parameterisation of $D \rightarrow V$ HFFs $\mathcal{D}_{V,\sigma}$ [58, 59] with $\sigma = 0, 1, 2, t$ respectively.

F_i	J^P	$m_{R,i}/\text{GeV}$
$\mathcal{D}_{V,t}$	0^-	1.864
$\mathcal{D}_{V,0;2}$	1^+	2.420
$\mathcal{D}_{V,1}$	1^-	2.007

servables for $D \rightarrow V(\rho, \omega, K^*)\ell^+\nu_\ell$ semileptonic decay mesons, and calculate the HFFs within the LCSR approach. In Section 3, after fixing the hadron input parameters for HFFs and extrapolating those HFFs to the whole q^2 region with SSE. Then, we apply it to investigate the $D \rightarrow V$ semileptonic decay physical observables, such as decay width, branching fraction and polarizations, and also compare our results with available experimental and other theoretical predictions. Finally, we briefly summary in Section 4.

2 Calculation Technology

2.1 $D \rightarrow V\ell^+\nu_\ell$ semileptonic decays

The $D \rightarrow V\ell^+\nu_\ell$ semileptonic decay process are displayed in Fig. 1, the detailed quarks transition can refer to the Table 1. The corresponding invariant matrix element can be expressed as follows:

$$\mathcal{M}(D \rightarrow V\ell^+\nu_\ell) = \frac{G_F}{\sqrt{2}} V_{cq}^* H^\mu L_\mu, \quad (2.1)$$

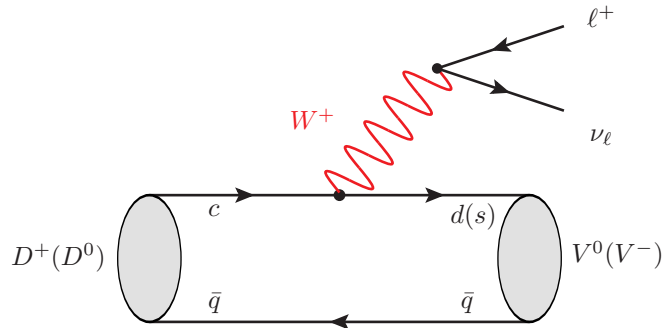


Figure 1. Typical diagram for the $D \rightarrow V\ell^+\nu_\ell$ semileptonic decay, where $q = u, d$ and $V = \rho, \omega, K^*$ mesons.

where fermi constant $G_F = 1.166 \times 10^{-5} \text{ GeV}^{-2}$, leptonic current $L_\mu = \bar{\nu}_\ell \gamma_\mu (1 - \gamma_5) \ell$ and the hadron matric element $H^\mu = \langle V|V^\mu - A^\mu|D \rangle$ with flavor-changing vector currents $V^\mu = \bar{q} \gamma^\mu c$ and axial-vector currents $A^\mu = \bar{q} \gamma^\mu \gamma_5 c$.

To get accurate polarization properties of the semileptonic decay $D \rightarrow V \ell^+ \nu_\ell$, one can decompose the hadron matric element H^μ into the HFFs by the off-shell W -boson polarization vectors. Specifically speaking,

$$\mathcal{D}_{V,\sigma}(q^2) = \sqrt{\frac{q^2}{\lambda}} \sum_{\alpha=0,\pm,t} \epsilon_\sigma^{*\mu}(q) \langle V(\tilde{p}, \tilde{\epsilon}_\alpha) | \bar{q} \gamma_\mu (1 - \gamma^5) c | D(p) \rangle, \quad (2.2)$$

where the standard kinematic function $\lambda = (t_- - q^2)(t_+ - q^2)$ with $t_\pm = (m_D \pm m_V)^2$ and $\epsilon_\sigma^{*\mu}(q)$ represent transverse ($\sigma = \pm$), longitudinal ($\sigma = 0$) or time-like ($\sigma = t$) polarization vectors. For the convenience of polarization research, two HFFs, $\mathcal{D}_{V,(1,2)}(q^2)$, are defined by a linear combinations of the transverse helicity projection vector, i.e. $\epsilon_{(1,2)}(q) = [\epsilon_-(q) \mp \epsilon_+(q)]/\sqrt{2}$. The detail HFFs calculation are shown in the next subsection.

The polar angle differential decay distribution in the momentum transfer squared, which is defined by the angle between $\vec{q} = \vec{p}_D - \vec{p}_V$ and the three-momentum of the charged lepton in the rest frame, can be written as follows,

$$\frac{d^2\Gamma}{dq^2 d \cos \theta} = \frac{|\mathbf{p}_V| v}{(2\pi)^3 32m_D^2} \sum_{\text{pol}} |\mathcal{M}|^2, \quad (2.3)$$

where $|\mathbf{p}_V| = \lambda^{1/2}/(2m_D^2)$, $v = (1 - m_\ell^2/q^2)$, and the covariant contraction $\sum_{\text{pol}} |\mathcal{M}|^2$ can be converted to a sum of bilinear products of hadronic HFFs and leptonic helicity amplitude by applying the completeness relation for the polarization four-vectors of the process. So the total differential decay width of $D \rightarrow V \ell \nu_\ell$ can be expressed as,

$$\begin{aligned} \frac{1}{|V_{cq}|^2} \frac{d\Gamma}{dq^2} &= \mathcal{G} \lambda^{3/2} v^2 \mathcal{D}_{\text{tot}} \\ &= \mathcal{G} \lambda^{3/2} v^2 \left[(1 + \delta_\ell) \sum \mathcal{D}_{V,i}^2 + 3\delta_\ell \mathcal{D}_{V,t}^2 \right], \end{aligned} \quad (2.4)$$

with $\delta_\ell = m_\ell^2/(2q^2)$, the parameter $\mathcal{G} = G_F^2/(192\pi^3 m_D^3)$, and variable i of the summation is taken as $i = 0, 1, 2$. The detailed expression reads,

$$\sum \mathcal{D}_{V,i}^2 = \mathcal{D}_{V,0}^2 + \mathcal{D}_{V,1}^2 + \mathcal{D}_{V,2}^2. \quad (2.5)$$

As we know that the total decay width can be separated into longitudinal and transverse part, i.e. $\Gamma = \Gamma^L + \Gamma^T$. The decay width for the vector meson longitudinal components Γ^L is defined as

$$\Gamma^L(q^2) = \mathcal{G} |V_{cq}|^2 \int_0^{q_{\text{max}}^2} dq^2 \lambda(q^2)^{3/2} \mathcal{D}_{V,0}^2(q^2) \quad (2.6)$$

and the decay width for the vector meson transverse components Γ^T is defined as

$$\Gamma^T(q^2) = \mathcal{G}|V_{cq}|^2 \int_0^{q_{\max}^2} dq^2 \lambda(q^2)^{3/2} \sum \mathcal{D}_{V,j}^2, \quad (2.7)$$

with the variable j of the summation is taken as $j = 1, 2$.

For the polarization properties of the semileptonic decay $D \rightarrow V\ell^+\nu_\ell$, one can study the longitudinal and transverse polarization firstly. Specifically, with the help of HFFs, the longitudinal P_L^ℓ and transverse P_T^ℓ polarization of the charged lepton in the final state and the longitudinal F_L^ℓ and transverse F_T^ℓ polarization fractions of the vector meson are given by:

$$\begin{aligned} P_L^\ell &= 1 - \frac{2 \sum \mathcal{D}_{V,i}^2}{\mathcal{D}_{\text{tot}}}, \\ P_T^\ell &= \frac{3\pi\sqrt{\delta_\ell}}{2\sqrt{2}} \frac{\mathcal{D}_{V,1}\mathcal{D}_{V,2} - \mathcal{D}_{V,0}\mathcal{D}_{V,t}}{\mathcal{D}_{\text{tot}}}, \\ F_L^\ell &= \frac{3\mathcal{D}_{V,t}^2\delta_\ell + (1 + \delta_\ell)\mathcal{D}_{V,0}^2}{\mathcal{D}_{\text{tot}}}, \\ F_T^\ell &= \frac{(1 + \delta_\ell)(\mathcal{D}_{V,1}^2 + \mathcal{D}_{V,2}^2)}{\mathcal{D}_{\text{tot}}}. \end{aligned} \quad (2.8)$$

And the forward-backward asymmetry $\mathcal{A}_{\text{FB}}^\ell$ can be written as,

$$\begin{aligned} \mathcal{A}_{\text{FB}}^\ell &= \frac{d\Gamma(F) - d\Gamma(B)}{d\Gamma(F) + d\Gamma(B)} \\ &= \frac{\int_0^1 d\cos\theta d\Gamma/d\cos\theta - \int_{-1}^0 d\cos\theta d\Gamma/d\cos\theta}{\int_0^1 d\cos\theta d\Gamma/d\cos\theta + \int_{-1}^0 d\cos\theta d\Gamma/d\cos\theta} \\ &= \frac{3}{2(1 + \delta_\ell)} \frac{2\delta_\ell\mathcal{D}_{V,0}\mathcal{D}_{V,t} - \mathcal{D}_{V,1}\mathcal{D}_{V,2}}{\sum \mathcal{D}_{V,i}^2 + \delta_\ell\mathcal{D}_{V,t}^2}. \end{aligned} \quad (2.9)$$

The lepton-side \mathcal{C}_F^ℓ convexity parameters has the form,

$$\mathcal{C}_F^\ell = -\frac{3}{4} \frac{(2\mathcal{D}_{V,0}^2 - \mathcal{D}_{V,1}^2 - \mathcal{D}_{V,2}^2)(1 - 2\delta_\ell)}{\mathcal{D}_{\text{tot}}}. \quad (2.10)$$

In order to make a comparison with other approaches, we take the same approach as the paper [60] to deal with the q^2 average of those observables. Specifically, if an observables A has the form $A = \mathcal{D}_x/\mathcal{D}_y$, one can multiply both the numerator and denominator the phase-space factor and then integrate the two separately. The detailed expression can be written as:

$$\langle A \rangle = \frac{\int C(q^2)\mathcal{D}_x dq^2}{\int C(q^2)\mathcal{D}_y dq^2}, \quad (2.11)$$

with q^2 dependence phase-space factor

$$C(q^2) = |\mathbf{p}\mathbf{v}| \frac{(q^2 - m_\ell^2)^2}{q^2}. \quad (2.12)$$

2.2 $D \rightarrow V$ HFFs

In order to derive LCSR for the four HFFs i.e. $\mathcal{D}_{V,\sigma}(q^2)$ with $\sigma = 0, 1, 2, t$, we first structure a two-point correlation function according to its strategies, as follows:

$$\Pi_\sigma(p, q) = i\sqrt{\frac{q^2}{\lambda}} \epsilon_\sigma^{*\mu}(q) \int d^4x e^{iq\cdot x} \langle V(\tilde{p}, \tilde{\epsilon}) | T\{j_{V,\mu}(x), j_D^\dagger(0)\} | 0 \rangle, \quad (2.13)$$

where the hadron vector and pseudoscalar current are $j_{V,\mu}(x) = \bar{q}(x)\gamma_\mu c(x)$ and $j_D^\dagger(0) = \bar{c}(0)i\gamma_5 u(0)$ respectively. Here the T is the product of the current operator.

In the timelike q^2 region, after inserting the complete intermediate states, which has the same quantum numbers $J^P = 0^-$ with the current operator $\bar{c}i\gamma_5 u$, into the hadron current of the correlation function, and further isolating the pole term of the lowest pseudoscalar D -meson, the correlation function can be read off:

$$\Pi_\sigma^H(p, q) = \sqrt{\frac{q^2}{\lambda}} \left[\frac{\epsilon_\sigma^{*\mu}(q) \langle V | \bar{q}\gamma_\mu c | D \rangle \langle D | \bar{c}i\gamma_5 u | 0 \rangle}{m_D^2 - (p+q)^2} + \sum_H \frac{\epsilon_\sigma^{*\mu}(q) \langle V | \bar{q}\gamma_\mu c | D^H \rangle \langle D^H | \bar{q}i\gamma_5 u | 0 \rangle}{m_{D^H}^2 - (p+q)^2} \right], \quad (2.14)$$

where $\langle D | \bar{c}i\gamma_5 u | 0 \rangle = m_D^2 f_D / m_c$. Replacing the sum of higher resonances and continuum states with the dispersion integrations, the hadronic representation for the correlator Π_σ^H finally have the form:

$$\Pi_\sigma^H(q^2, (p+q)^2) = \frac{m_D^2 f_D}{m_c [m_D^2 - (p+q)^2]} \mathcal{D}_\sigma(q^2) + \int_{s_0}^\infty \frac{\rho_\sigma^H(s)}{s - (p+q)^2} ds + \text{subtractions}, \quad (2.15)$$

where s_0 is an “internal” parameters of LCSR.

In the spacelike q^2 region, e.g. $(p+q)^2 - m_c^2 \ll 0$, and $q^2 \ll m_c^2 - \mathcal{O}(1\text{GeV}^2)$, one need to contract the c -quark operator by applying a free c -quark propagator:

$$\begin{aligned} \langle 0 | c_\alpha^i(x) \bar{c}_\beta^j(0) | 0 \rangle &= -i \int \frac{d^4k}{(2\pi)^4} e^{-ik\cdot x} \left\{ \delta^{ij} \frac{\not{k} + m_c}{m_c^2 - k^2} + g_s \int_0^1 dv G^{\mu\nu\alpha}(vx) \left(\frac{\lambda}{2} \right)^{ij} \right. \\ &\quad \times \left. \left[\frac{\not{k} + m_c}{2(m_c^2 - k^2)^2} \sigma_{\mu\nu} + \frac{1}{m_c^2 - k^2} vx_\mu \gamma_\nu \right] \right\}_{\alpha\beta}. \end{aligned} \quad (2.16)$$

For further OPE treatment, one need the nonlocal matrix elements, which are convoluted with the meson light-cone distribution amplitudes (LCDAs) of growing twist:

$$\langle V(\tilde{p}, \tilde{\epsilon}) | \bar{q}_1(x) \sigma_{\mu\nu} q_2(0) | 0 \rangle = -i f_V^\perp \int_0^1 du e^{iu(\tilde{p}\cdot x)} \left\{ (\tilde{\epsilon}_\mu^* \tilde{p}_\nu - \tilde{\epsilon}_\nu^* \tilde{p}_\mu) \left[\phi_{2;V}^\perp(u) + \frac{m_V^2 x^2}{4} \phi_{4;V}^\perp(u) \right] \right\}$$

$$\begin{aligned}
& + (\tilde{p}_\mu x_\nu - \tilde{p}_\nu x_\mu) \frac{\tilde{\epsilon}^* \cdot x}{(\tilde{p} \cdot x)^2} m_V^2 \left[\phi_{3;V}^\parallel(u) - \frac{1}{2} \phi_{2;V}^\perp(u) - \frac{1}{2} \psi_{4;V}^\perp(u) \right] \\
& + \frac{1}{2} (\tilde{\epsilon}_\mu^* x_\nu - \tilde{\epsilon}_\nu^* x_\mu) \frac{m_V^2}{\tilde{p} \cdot x} \left[\psi_{4;V}^\perp(u) - \phi_{2;V}^\perp(u) \right] \Big\} , \tag{2.17}
\end{aligned}$$

$$\langle V(\tilde{p}, \tilde{\epsilon}) | \bar{q}_1(x) q_2(0) | 0 \rangle = -\frac{i}{2} f_V^\perp (\tilde{\epsilon}^* \cdot x) m_V^2 \int_0^1 du e^{iu(\tilde{p} \cdot x)} \psi_{3;V}^\parallel(u) , \tag{2.18}$$

$$\begin{aligned}
\langle V(\tilde{p}, \tilde{\epsilon}) | \bar{q}_1(x) \gamma_\mu q_2(0) | 0 \rangle = m_V^2 f_V^\parallel \int_0^1 du e^{iu(\tilde{p} \cdot x)} & \left\{ \frac{\tilde{\epsilon}^* \cdot x}{\tilde{p} \cdot x} \tilde{p}_\mu \left[\phi_{2;V}^\parallel(u) + \frac{m_V^2 x^2}{4} \phi_{4;V}^\parallel(u) \right] \right. \\
& + \left(\tilde{\epsilon}_\mu^* - \tilde{p}_\mu \frac{\tilde{\epsilon}^* \cdot x}{p \cdot x} \right) \phi_{3;V}^\perp(u) - \frac{1}{2} m_V^2 x_\mu \frac{\tilde{\epsilon}^* \cdot x}{(\tilde{p} \cdot x)^2} \left[\psi_{4;V}^\parallel(u) + \phi_{2;V}^\parallel(u) \right. \\
& \left. \left. - 2 \phi_{3;V}^\perp(u) \right] \right\} , \tag{2.19}
\end{aligned}$$

$$\langle V(\tilde{p}, \tilde{\epsilon}) | \bar{q}_1(x) \gamma_\mu \gamma_5 q_2(0) | 0 \rangle = -\frac{1}{4} m_V f_V^\parallel \varepsilon^{\mu\nu\alpha\beta} \tilde{\epsilon}_\mu^* \tilde{p}_\alpha x_\beta \int_0^1 du e^{iu(\tilde{p} \cdot x)} \psi_{3;V}^\perp(u) , \tag{2.20}$$

where $V = \rho, \omega, K^*$ mesons and $q_1 = d(s)$ for ρ, ω, K^* mesons.

After replacing those hadronic matrix elements and subtracting the contribution of the continuum spectrum by using dispersion integration, one can finish the QCD representation calculation. In this paper, we will not consider the three-particle part due to its negligible contribution. Specifically, it is no more than 0.3% of the total TFFs, and a more detailed analysis can be obtained from our previous study [61].

Moreover, one need to equate the two types of representation of correlator and subtract the contributions from higher resonances and continuum states. With the help of Borel transformation, the LCSR for $D \rightarrow V$ HFFs can be finally read off:

$$\begin{aligned}
\mathcal{D}_{V,0}(q^2) = \int_0^1 du e^{(m_D^2 - s)/M^2} & \frac{m_c f_V^\perp \mathcal{F}}{2\sqrt{\lambda} m_V m_D^2 f_D} \left\{ 2\mathcal{S}\Theta(c(u, s_0)) \phi_{2;V}^\perp(u) - \frac{\lambda m_c m_V \tilde{f}_V}{u^2 M^2} \tilde{\Theta}(c(u, s_0)) \right. \\
& \times \Phi_{2;V}^\parallel(u) - (\tilde{m}_q m_V \tilde{f}_V - m_V^2) \left[\mathcal{F}\Theta(c(u, s_0)) - \lambda \frac{1}{u M^2} \tilde{\Theta}(c(u, s_0)) \right] \psi_{3;V}^\parallel(u) + m_c m_V \\
& \times \tilde{f}_V \left[\frac{\lambda}{u^2 M^2} \tilde{\Theta}(c(u, s_0)) \Phi_{3;V}^\perp(u) + \mathcal{F}\Theta(c(u, s_0)) \phi_{3;V}^\perp(u) \right] + m_V^2 \mathcal{S} \left[\frac{\mathcal{N}}{2u^3 M^4} \tilde{\tilde{\Theta}}(c(u, s_0)) \right. \\
& \left. - \frac{3}{2u^2 M^2} \tilde{\Theta}(c(u, s_0)) \right] \phi_{4;V}^\perp(u) - \left[\frac{\lambda \mathcal{S}}{2u^3 M^4} \tilde{\tilde{\Theta}}(c(u, s_0)) - m_V^2 \frac{\mathcal{S} - 4\lambda}{u^2 M^2} \right] \tilde{\Theta}(c(u, s_0)) I_L(u) \\
& - \frac{\lambda m_c^3 m_V^3 \tilde{f}_V}{u^4 M^6} \tilde{\tilde{\Theta}}(c(u, s_0)) \Phi_{4;V}^\perp(u) + m_c m_V^3 \tilde{f}_V \left[\frac{\lambda}{u^2 M^4} \tilde{\tilde{\Theta}}(c(u, s_0)) + \frac{\mathcal{F}}{u^2 M^2} \tilde{\Theta}(c(u, s_0)) \right] \\
& \times C_V(u) - m_V^2 \left[\frac{3}{2} \Theta(c(u, s_0)) + \left(\frac{\mathcal{N}}{u^2 M^2} - \frac{\lambda}{2u M^2 \mathcal{F}} \right) \tilde{\Theta}(c(u, s_0)) \right] H_3(u) , \tag{2.21}
\end{aligned}$$

$$\begin{aligned} \mathcal{D}_{V,1}(q^2) = & \int_0^1 du e^{(m_D^2-s)/M^2} \frac{m_c f_V^\perp \sqrt{2q^2}}{2m_D^2 f_D} \left\{ \Theta(c(u, s_0)) \phi_{2;V}^\perp(u) + m_V^2 \left[\frac{\mathcal{N}}{u^3 M^4} \tilde{\Theta}(c(u, s_0)) + \frac{3}{u^2 M^2} \right. \right. \\ & \left. \times \tilde{\Theta}(c(u, s_0)) \right] \phi_{4;V}^\perp(u) - \frac{m_V m_c \tilde{f}_V}{2u^2 M^2} \tilde{\Theta}(c(u, s_0)) \psi_{3;V}^\perp(u) \left. \right\}, \end{aligned} \quad (2.22)$$

$$\begin{aligned} \mathcal{D}_{V,2}(q^2) = & \int_0^1 du e^{(m_D^2-s)/M^2} \frac{\sqrt{2q^2} m_c f_V^\perp}{2\sqrt{\lambda} m_D^2 f_D} \left\{ \mathcal{E} \Theta(c(u, s_0)) \phi_{2;V}^\perp(u) - 2 \Theta(c(u, s_0)) (\tilde{f}_V m_V \tilde{m}_q \right. \\ & - m_V^2) \psi_{3;V}^\parallel(u) + m_V^2 \mathcal{E} \left[\frac{\mathcal{N}}{u^3 M^4} \tilde{\Theta}(c(u, s_0)) + \frac{3}{u^2 M^2} \tilde{\Theta}(c(u, s_0)) \right] \phi_{4;V}^\perp(u) + \frac{2m_V^2}{u^2 M^2} \\ & \times \mathcal{E} \tilde{\Theta}(c(u, s_0)) I_L(u) - m_V^2 \left[3 \Theta(c(u, s_0)) + \frac{2\mathcal{N}}{u^2 M^2} \tilde{\Theta}(c(u, s_0)) \right] H_3(u) - 2m_c \tilde{f}_V m_V \\ & \times \Theta(c(u, s_0)) \phi_{3;V}^\perp(u) - \frac{2m_c m_V^3 \tilde{f}_V}{u^2 M^2} \tilde{\Theta}(c(u, s_0)) C_V(u) \left. \right\}, \end{aligned} \quad (2.23)$$

$$\begin{aligned} \mathcal{D}_{V,t}(q^2) = & \int_0^1 du e^{(m_D^2-s)/M^2} \frac{m_c m_V f_V^\perp}{2m_V m_D^2 f_D} \left\{ u m_V \Theta(c(u, s_0)) \phi_{2;V}^\perp(u) - \frac{m_c \tilde{f}_V \mathcal{F}}{u^2 M^2} \tilde{\Theta}(c(u, s_0)) \right. \\ & \times \Phi_{2;V}^\parallel(u) - (\tilde{m}_q \tilde{f}_V - m_V) \left[\Theta(c(u, s_0)) + \frac{u \mathcal{F} + 2q^2}{u^2 M^2} \tilde{\Theta}(c(u, s_0)) \right] \psi_{3;V}^\parallel(u) - m_c \tilde{f}_V \\ & \times \Theta(c(u, s_0)) \phi_{3;V}^\perp(u) + m_c \tilde{f}_V \frac{\mathcal{F}}{u^2 M^2} \tilde{\Theta}(c(u, s_0)) \Phi_{3;V}^\perp(u) + m_V^3 \left[\frac{\mathcal{N}}{u^2 M^4} \tilde{\Theta}(c(u, s_0)) \right. \\ & \left. + \frac{3}{u M^2} \tilde{\Theta}(c(u, s_0)) \right] \phi_{4;V}^\perp(u) + m_c^3 m_V^2 \tilde{f}_V \frac{\mathcal{F}}{u^4 M^6} \tilde{\tilde{\Theta}}(c(u, s_0)) \Phi_{4;V}^\parallel(u) - m_V \left[\frac{\mathcal{E}}{2u M^2} \right. \\ & \times \tilde{\Theta}(c(u, s_0)) + \frac{3}{2} \Theta(c(u, s_0)) \left. \right] H_3(u) - m_V \left[\frac{9\mathcal{F} - 2u m_V^2 + 15q^2}{u^2 M^2} \tilde{\Theta}(c(u, s_0)) + \frac{\mathcal{W}}{u^3 M^4} \right. \\ & \times \tilde{\tilde{\Theta}}(c(u, s_0)) \left. \right] I_L(u) + \frac{m_c \tilde{f}_V}{2} \left[\frac{2m_V^2}{u^2 M^2} \tilde{\Theta}(c(u, s_0)) + \frac{\mathcal{S}}{u^3 M^4} \tilde{\tilde{\Theta}}(c(u, s_0)) \right] C_V(u) \left. \right\}, \end{aligned} \quad (2.24)$$

where $\mathcal{E} = m_D^2 + \xi m_V^2 - q^2$, $\mathcal{F} = m_D^2 - m_V^2 - q^2$, $\mathcal{N} = u m_D^2 - u \bar{u} m_V^2 + \bar{u} q^2$, $\mathcal{S} = 2m_V^2 (u m D^2 - u m_V^2 + (1 - \bar{u}) q^2)$, $\mathcal{W} = 2m_D^2 [-u \xi m_V^2 + q^2 (1 + u + u \bar{u})] + u \xi (m_D^4 + m_V^4) - 2q^2 (1 + u) \bar{u} m_V^2 - q^4 (2 + u)$ and $s = [m_b^2 - \bar{u} (q^2 - u m_V^2)]/u$ with $\bar{u} = 1 - u$, $\xi = 2u - 1$. The effective decay constant $\tilde{f}_V = f_V^\parallel / f_V^\perp$ and simplified distribution functions $\Phi_{2;V}^\parallel(u)$, $\Phi_{3;V}^\perp(u)$, $\Phi_{4;V}^\perp(u)$, $I_L(u)$ and $H_3(u)$ are defined as

$$\begin{aligned} \Phi_{2;V}^\parallel(u) &= \int_0^u dv \phi_{2;V}^\parallel(u), \\ \Phi_{3;V}^\perp(u) &= \int_0^u dv \phi_{3;V}^\perp(u), \\ \Phi_{4;V}^\perp(u) &= \int_0^u dv \phi_{4;V}^\perp(u), \end{aligned}$$

$$\begin{aligned}
H_3(u) &= \int_0^u dv \left[\psi_{4;V}^\perp(v) - \phi_{2;V}^\perp(v) \right], \\
I_L(u) &= \int_0^u dv \int_0^v dw \left[\phi_{3;V}^\parallel(w) - \frac{1}{2} \phi_{2;V}^\perp(w) - \frac{1}{2} \psi_{4;V}^\perp(w) \right], \\
C_V(u) &= \int_0^u dv \int_0^v dw \left[\psi_{4;V}^\parallel(w) + \phi_{2;V}^\parallel(w) - 2\phi_{3;V}^\perp(w) \right]. \tag{2.25}
\end{aligned}$$

The $\Theta(c(u, s_0))$ is conventional step function, $\widetilde{\Theta}[c(u, s_0)]$ and $\widetilde{\widetilde{\Theta}}(c(u, s_0))$ are defined as

$$\int_0^1 \frac{du}{u^2 M^2} e^{-s/M^2} \widetilde{\Theta}(c(u, s_0)) f(u) = \int_{u_0}^1 \frac{du}{u^2 M^2} e^{-s/M^2} f(u) + \delta(c(u_0, s_0)), \tag{2.26}$$

$$\int_0^1 \frac{du}{2u^3 M^4} e^{-s/M^2} \widetilde{\widetilde{\Theta}}(c(u, s_0)) f(u) = \int_{u_0}^1 \frac{du}{2u^3 M^4} e^{-s/M^2} f(u) + \Delta(c(u_0, s_0)), \tag{2.27}$$

where

$$\begin{aligned}
\delta(c(u, s_0)) &= e^{-s_0/M^2} \frac{f(u_0)}{\mathcal{C}_0}, \\
\Delta(c(u, s_0)) &= e^{-s_0/M^2} \left[\frac{1}{2u_0 M^2} \frac{f(u_0)}{\mathcal{C}_0} - \frac{u_0^2}{2\mathcal{C}_0} \frac{d}{du} \left(\frac{f(u)}{u\mathcal{C}} \right) \Big|_{u=u_0} \right],
\end{aligned}$$

$\mathcal{C}_0 = m_b^2 + u_0^2 m_V^2 - q^2$ and u_0 is the solution of $c(u_0, s_0) = 0$ with $0 \leq u_0 \leq 1$. Numerically, we observe that the leading-twist terms are dominant for the LCSR of the HFFs, agreeing well with the usual δ -power counting rule. Thus, those HFFs shall provide us a useful platform in testing the properties of the leading-twist LCDAs via comparisons with the data or predictions from other theoretical approaches.

3 Numerical Analysis

In order to doing the numerical analysis, the input parameters are taken as follows. The mass of meson are $m_D = 1.865$ GeV, $m_\rho = 0.775$ GeV, $m_\omega = 0.782$ GeV and $m_{K^*} = 0.892$ GeV. The c -quark pole mass $m_c = 1.28(3)$ GeV is taken from the particle data group [59]. For the decay constant we take $f_D = 0.204(5)$ for D meson, $f_\rho^\parallel = 0.198(7)$ and $f_\rho^\perp = 0.160(10)$ for ρ meson, $f_\omega^\parallel = 0.195(3)$ and $f_\omega^\perp = 0.145(10)$ for ω meson, $f_{K^*}^\parallel = 0.226(28)$ and $f_{K^*}^\perp = 0.185(10)$ for K^* meson [52]. The Cabibbo-Kobayashi-Maskawa matrix element $|V_{cd}| = 0.216$ and $|V_{cs}| = 0.997$.

3.1 LCDAs and $D \rightarrow V$ HFFs

Within the QCD LCSR framework, HFFs will be expressed by different twist LCDAs like TFFs, due to the same method OPE for handling correlation function. The resultant HFFs contain twist-2, twist-3, and twist-4 terms. In the following, we will discuss the associated LCDAs and parameters.

For the leading twist LCDAs, its conformal expansion can be expressed in terms of Gegenbauer polynomials,

$$\phi_{2;V}^{\parallel,\perp}(u, \mu^2) = \phi_{\text{asy}}(u) \left[1 + \sum a_n(\mu^2) C_n^{3/2}(\xi) \right]. \quad (3.1)$$

The $\phi_{\text{asy}}(u) = 6u\bar{u}$ stand for the asymptotic DA. The $\phi_{2;V}^{\parallel,\perp}(u, \mu^2)$ will equals to $\phi_{\text{asy}}(u)$ in the limit $\mu^2 \rightarrow \infty$. Due to the $D \rightarrow V$ with $V = \rho, \omega, K^*$ mesons HFFs were studied for the first time in order to make a comparison with other theoretical and experimental predictions, we take the twist-2,3,4 LCDAs' moments and coupling constants given by P. Ball [62], which are calculated within SVZ QCD sum rule taken by many theoretical groups. The analytical expression and values are listed in the Appendix.

Then, there are two internal parameters, i.e. continuum threshold s_0 and Borel windows M^2 . The former is a demarcation for the D -meson ground state and higher mass contributions. Specifically, we take the continuum thresholds $s_0(\text{GeV}^2)$ for $D \rightarrow V$ HFFs $\mathcal{D}_{V,0}(q^2)$, $\mathcal{D}_{V,1}(q^2)$, $\mathcal{D}_{V,2}(q^2)$ and $\mathcal{D}_{V,t}(q^2)$ as: $s_{\rho,0} = 4.0(3)$, $s_{\rho,1} = 4.0(3)$, $s_{\rho,2} = 4.0(3)$, $s_{\rho,t} = 4.5(3)$, $s_{\omega,0} = 3.6(3)$, $s_{\omega,1} = 6.5(3)$, $s_{\omega,2} = 4.0(3)$, $s_{\omega,t} = 4.0(3)$, $s_{K^*,0} = 4.0(3)$, $s_{K^*,1} = 6.0(3)$, $s_{K^*,2} = 4.0(3)$ and $s_{K^*,t} = 3.7(3)$.

To determine the Borel parameters for the $D \rightarrow V$ HFFs LCSR, we adopt the following three criteria:

- We require the continuum contribution to be less than 35% of the total LCSR.
- We require all the high-twist LCDAs' contributions to be less than 15% of the total LCSR.
- The derivatives of LCSR for HFFs with respect to $(-1/M^2)$ give four LCSR for the D -meson mass m_D . We require the predicted D -meson mass to be fulfilled in comparing with the experiment one, i.e. $|m_D^{\text{th}} - m_D^{\text{exp}}|/m_D^{\text{exp}} \leq 0.1\%$.

Thus, the obtained Borel windows $M^2(\text{GeV}^2)$ are: $M_{\rho,0}^2 = 2.5(3)$, $M_{\rho,1}^2 = 4.0(3)$, $M_{\rho,2}^2 = 3.5(3)$, $M_{\rho,t}^2 = 3.0(3)$, $M_{\omega,0}^2 = 2.5(3)$, $M_{\omega,1}^2 = 4.8(3)$, $M_{\omega,2}^2 = 3.0(3)$, $M_{\omega,t}^2 = 3.0(3)$, $M_{K^*,0}^2 = 2.5(3)$, $M_{K^*,1}^2 = 6.0(3)$, $M_{K^*,2}^2 = 4.0(3)$ and $M_{K^*,t}^2 = 2.7(3)$.

The reliable regions for the D -meson semileptonic decays within LCSR approach can be set to $0 \leq q^2 \leq q_{\text{LCSR,max}}^2 \approx 0.8 \text{ GeV}^2$. Meanwhile, the allowable physical range of the momentum transfer is $0 \leq q^2 \leq q_{V,\text{max}}^2$ with

$$\begin{aligned} q_{\rho,\text{max}}^2 &= (m_D - m_\rho)^2 \simeq 1.18 \text{ GeV}^2, \\ q_{\omega,\text{max}}^2 &= (m_D - m_\omega)^2 \simeq 1.17 \text{ GeV}^2, \\ q_{K^*,\text{max}}^2 &= (m_D - m_{K^*})^2 \simeq 0.98 \text{ GeV}^2, \end{aligned}$$

for ρ , ω and K^* mesons, respectively. In the following, we use the Simplified Series Expansion to do the extrapolation for the HFFs based on the analyticity and unitarity consideration.

Table 3. The fitted parameters $a_{0;1;2}^V$ for the HFFs $\mathcal{D}_{V,\sigma}$, where all input parameters are set to be their central values.

	$\mathcal{D}_{V,0}$	$\mathcal{D}_{V,1}$	$\mathcal{D}_{V,2}$	$\mathcal{D}_{V,t}$
a_0^ρ	1.841	1.187	4.257	0.913
a_1^ρ	-68.95	-5.177	-137.2	-18.49
a_2^ρ	-879.8	-88.14	1774	160.2
Δ_ρ	0.000	0.008	0.042	0.000
a_0^ω	1.786	0.763	4.666	0.868
a_1^ω	-68.41	-1.125	-162.6	-18.46
a_2^ω	883.8	-22.53	2163	170.1
Δ_ω	0.000	0.001	0.050	0.000
$a_0^{K^*}$	1.937	0.941	5.074	0.975
$a_1^{K^*}$	-91.04	2.976	-209.4	-21.97
$a_2^{K^*}$	1438	-70.30	3545	181.0
Δ_{K^*}	0.000	0.001	0.031	0.000

The extrapolation of the HFFs satisfies the following parameterized formula,

$$\mathcal{D}_{V,0}(t) = \frac{1}{B(t)\sqrt{z(t,t_-)\phi_T^{V-A}(t)}} \sum_{k=0,1,2} a_k^{V,0} z^k, \quad (3.2)$$

$$\mathcal{D}_{V,1}(t) = \frac{\sqrt{-z(t,0)}}{B(t)\phi_T^{V-A}(t)} \sum_{k=0,1,2} a_k^{V,1} z^k, \quad (3.3)$$

$$\mathcal{D}_{V,2}(t) = \frac{\sqrt{-z(t,0)}}{B(t)\sqrt{z(t,t_-)\phi_T^{V-A}(t)}} \sum_{k=0,1,2} a_k^{V,2} z^k, \quad (3.4)$$

$$\mathcal{D}_{V,t}(t) = \frac{1}{B(t)\phi_L^{V-A}(t)} \sum_{k=0,1,2} a_k^{V,t} z^k, \quad (3.5)$$

where $\phi_I^X(t) = 1$, $\sqrt{-z(t,0)} = \sqrt{q^2}/m_D$, $B(t) = 1 - q^2/m_\sigma^2$, $\sqrt{z(t,t_-)} = \sqrt{\lambda}/m_D^2$, and

$$z(t) = \frac{\sqrt{t_+ - t} - \sqrt{t_+ - t_0}}{\sqrt{t_+ - t} + \sqrt{t_+ - t_0}}$$

with $t_\pm = (m_D \pm m_V)^2$ and $t_0 = t_+(1 - \sqrt{1 - t_-/t_+})$.

The parameters a_k^σ can be determined by requiring the “quality” of fit (Δ_V) to be less than one, which is defined as

$$\Delta_V = \frac{\sum_t |\mathcal{D}_{V,\sigma}(t) - \mathcal{D}_{V,\sigma}^{\text{fit}}(t)|}{\sum_t |\mathcal{D}_{V,\sigma}(t)|} \times 100, \quad (3.6)$$

Table 4. The total decay widths $\Gamma/|V_{cq}|^2$, $\Gamma^L/|V_{cq}|^2$ and $\Gamma^T/|V_{cq}|^2$ (in the unit $10^{-15} \text{ GeV}^{-1}$) for the central value.

	$\Gamma/ V_{cq} ^2$	$\Gamma^L/ V_{cq} ^2$	$\Gamma^T/ V_{cq} ^2$
$D \rightarrow \rho \ell^+ \nu_\ell$	49.564	26.299	23.265
$D \rightarrow \omega \ell^+ \nu_\ell$	44.108	23.320	20.788
$D \rightarrow K^* \ell^+ \nu_\ell$	33.631	18.539	15.092

where $t \in [0, 0.02, \dots, 0.58, 0.8] \text{ GeV}^2$. We put the determined parameters $a_k^{V,\sigma}$ in Table 3, in which all the input parameters are set to be their central values.

The extrapolated HFFs in whole q^2 -region are presented in the Fig. 2, where the shaded bands are uncertainties from various input parameters. The HFFs of the three vector mesons are corresponding similar due to the same analytic expression, Eqs. (2.21)–(2.24) and small different parameter values. We can see $\mathcal{D}_{V,(1;2)} = 0$ at $q^2 = 0 \text{ GeV}^2$, which are caused by the coefficient q^2 of $\mathcal{D}_{V,(1;2)}(q^2)$. The q^2 coefficient also depresses the error of HFFs $\mathcal{D}_{V,(1;2)}(q^2)$ for the smaller q^2 , which can be directly seen from this figure. Meanwhile, this depresses effect can be directly transmitted to the differential transversal decay width in Fig. 3 seen in the next subsection.

3.2 D Meson Semileptonic Decays

The HFFs extracted from the LCSR are employed to study the D -meson semileptonic decay, i.e. the decay width, branching fractions, longitudinal and transverse polarization, forward-backward asymmetry and lepton-side convexity parameter, which is frequently used for precision test the SM and searching of new physics beyond SM.

3.2.1 Decay width

In this part, we probe the decay width of $D \rightarrow V$ semilepton decay by applying the Eqs. (2.4), (2.6) and (2.7). Firstly, we present the LCSR predictions for the polarization differential decay widths $1/|V_{cq}|^2 \times d\Gamma^L/dq^2$, $1/|V_{cq}|^2 \times d\Gamma^T/dq^2$ and the total differential decay widths $1/|V_{cq}|^2 \times d\Gamma/dq^2$ in Fig. 3, in which the dashed, dotted and solid line represent the corresponding central values, the uncertainties are coming from the squared average of all input parameters.

For the central value in the Fig. 3, we find that there is similar behavior for all of the differential decay width with $|V_{cq}|$ independent for $D \rightarrow V \ell^+ \nu_\ell$ semileptonic decays. Both the total differential width and transversal differential width increase first and then decrease with q^2 . The longitudinal differential width is almost unchanged in the small to middle q^2 region, while it drops sharply in the large q^2 region. Besides, the longitudinal differential width is dominant in small q^2 region, while the transversal differential width is dominant in large q^2 region. The dominant alternate points are located near the midpoint of the whole physical region, which are represented by red star in Fig. 3, i.e $q_{\text{mix},(\rho,\omega,K^*)}^2 = (0.51, 0.54, 0.49) \text{ GeV}^2$.

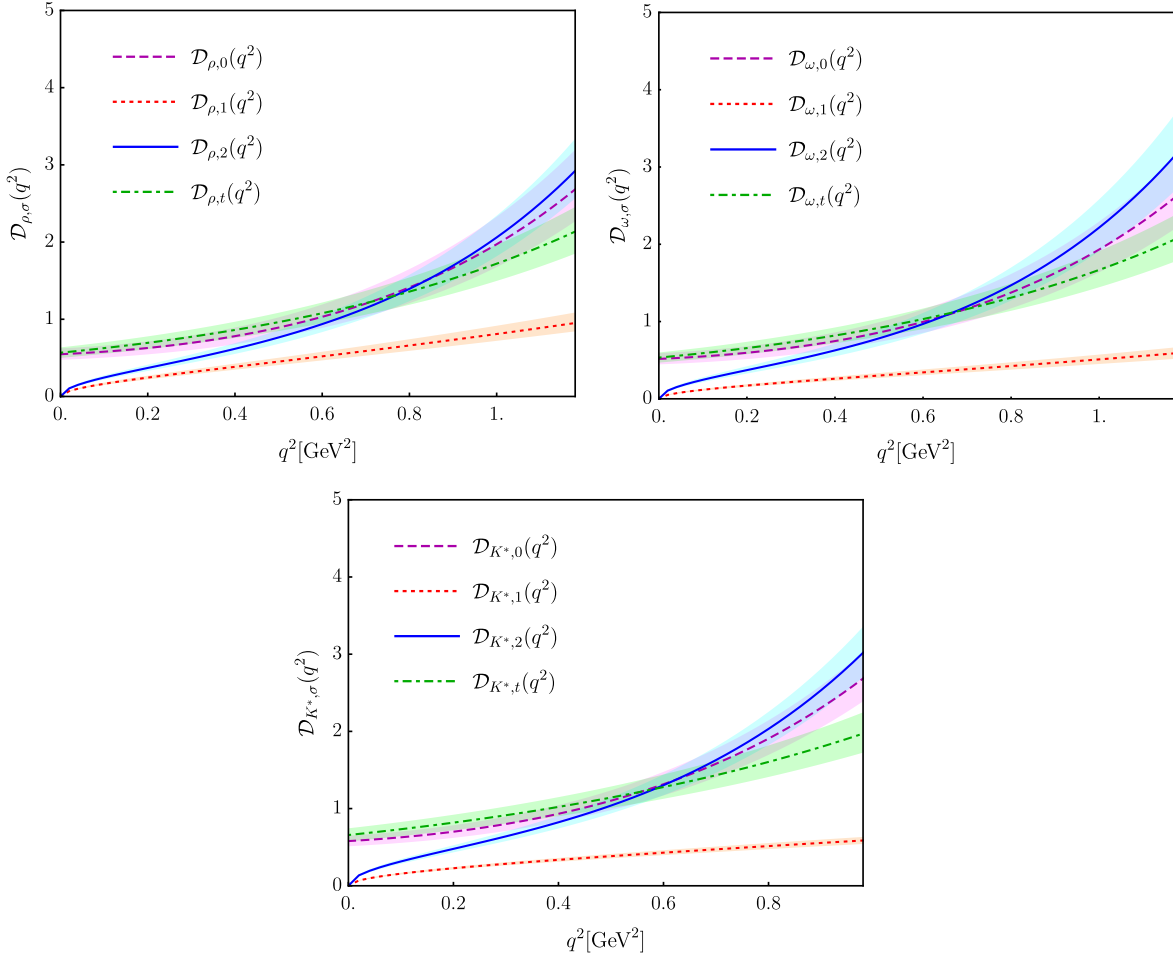


Figure 2. The extrapolated LCSR predictions HFFs $\mathcal{D}_{V,\sigma}(q^2)$ for the $D \rightarrow V$ with $V = \rho, \omega, K^*$ mesons. The solid lines represent the center values and the shaded bands corresponds to their uncertainties. The maximum extrapolated physically allowable point q^2 are $q_{\rho,\text{max}}^2 = (m_D - m_\rho)^2 \simeq 1.18 \text{ GeV}^2$, $q_{\omega,\text{max}}^2 = (m_D - m_\omega)^2 \simeq 1.17 \text{ GeV}^2$ and $q_{K^*,\text{max}}^2 = (m_D - m_{K^*})^2 \simeq 0.98 \text{ GeV}^2$ for ρ, ω and K^* mesons, respectively.

The three figures imply that the total width decreases as the mass of the final meson increases, which is intuitive from Table 4. There are three main reasons for this conclusion:

- (i) The physically feasible region decreases from the left to right, which caused by the increasing mass of final meson;
- (ii) It is decreased for the peak of the longitudinal and transversal differential width from the left to right;
- (iii) The curve trend for longitudinal and transverse differential width is nearly the same.

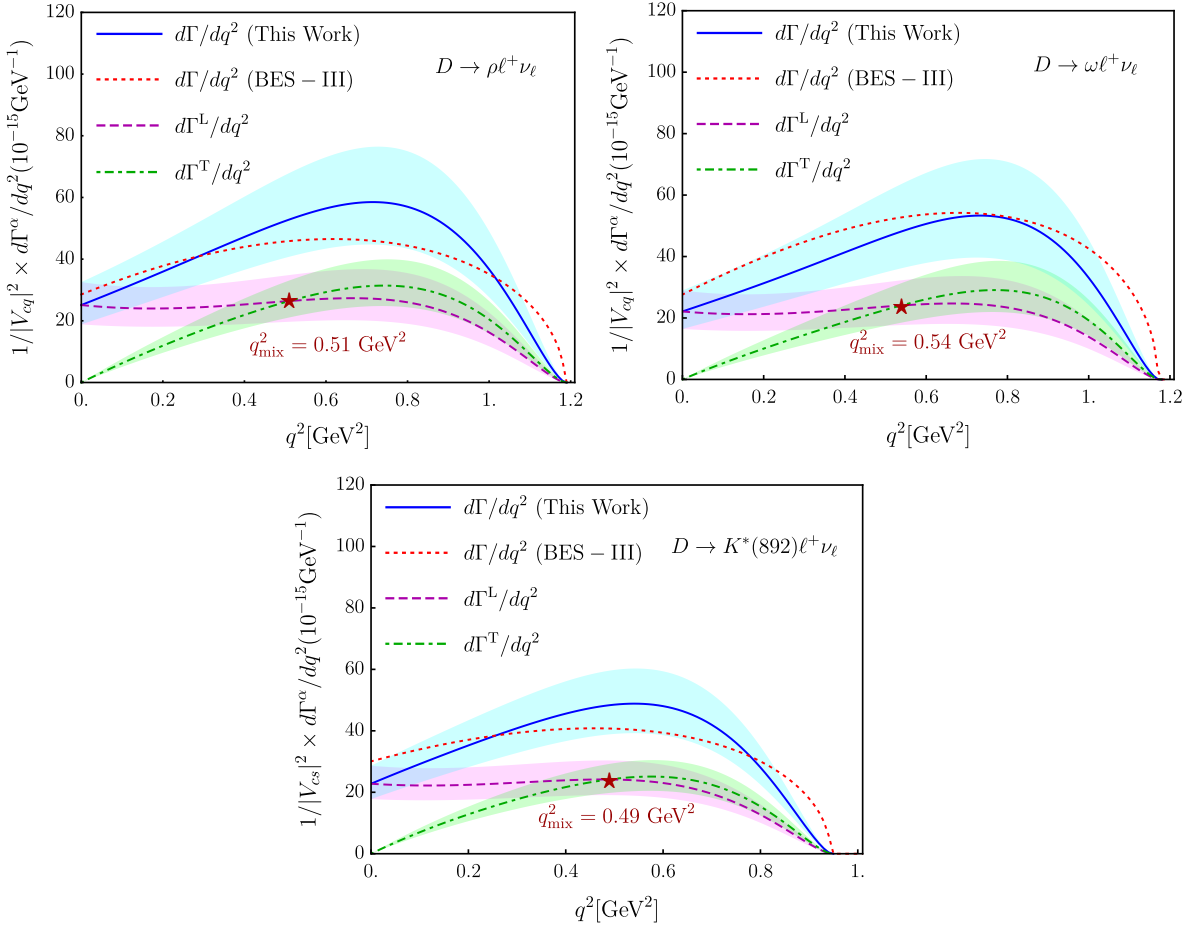


Figure 3. the LCSR predictions for the polarized differential decay widths $1/|V_{cq}|^2 \times d\Gamma^{\text{L,T}}/dq^2$ and the total differential decay widths $1/|V_{cq}|^2 \times d\Gamma/dq^2$ for $\rho, \omega, K^*(892)$ mesons, in which the dashed, dotted and solid line represent the corresponding central values, and the shaded band are the squared average of all the input parameters. As a comparison, we also present the BES-III predictions.

For comparison, the central value of the total differential width of BES-III is also shown in the Fig. 3. We find that the curve of BES-III is in agreement with our prediction in errors. But there is a significantly different for the shape of the center curve, especially for the large q^2 region. The main reason is that BES-III use the unipolar point continuation formula, while HFFs need to use the SSE formula.

Then we show the total decay widths $\Gamma/|V_{cq}|^2$, $\Gamma^{\text{L}}/|V_{cq}|^2$ and $\Gamma^{\text{T}}/|V_{cq}|^2$ in the Table 4. The three kinds of total decay widths are decreases as the mass of the final meson increases, which is consistent with Fig. 3. There is also an interesting phenomenon: it is almost identical for both total decay widths $\Gamma^{\text{L}}/|V_{cq}|^2$ and $\Gamma^{\text{T}}/|V_{cq}|^2$ gaps between different decay channels. We list the ratio $\Gamma^{\text{L}}/\Gamma^{\text{T}}$ for the $D \rightarrow V \ell^+ \nu_\ell$ semileptonic decays in the Table 5. As a comparison, we

Table 5. Ratio Γ^L/Γ^T for the $D \rightarrow V(\rho, \omega, K^*)\ell^+\nu_\ell$ semileptonic decays, where the uncertainties are the squared average of all the input parameters. The theoretical and lattice results in references are listed as a comparison.

	This work	CCQM [60]	CQM [63]	LCSR[64]	QCDSR[65]	LQCD[66]
$D \rightarrow \rho e^+\nu_e$	$1.130^{+0.095}_{-0.133}$	1.13		1.16	1.17(9)	0.86(6)
$D \rightarrow \rho \mu^+\nu_\mu$	$1.119^{+0.095}_{-0.132}$	1.04				-
$D \rightarrow \omega e^+\nu_e$	$1.122^{+0.042}_{-0.075}$	1.10	-	-	-	-
$D \rightarrow \omega \mu^+\nu_\mu$	$1.110^{+0.042}_{-0.074}$	1.02	-	-	-	-
$D \rightarrow K^* e^+\nu_e$	$1.228^{+0.061}_{-0.074}$	1.18		1.28	1.15(10)	
$D \rightarrow K^* \mu^+\nu_\mu$	$1.212^{+0.060}_{-0.073}$	1.07	-	-	-	1.2(3)

also present other theoretical predictions, i.e. CCQM [60], CQM [63], LCSR [64], QCDSR [65] and LQCD [66]. All of our predictions for the ratio Γ^L/Γ^T agree with that of the CCQM within errors. Although the rest of the theoretical predictions are incomplete for this ratio Γ^L/Γ^T , again, our results are in good agreement with them within the margin of error, except for QCDSR results.

As a further step, we calculate the branching fractions of $D \rightarrow V\ell^+\nu_\ell$ by employing $\tau(D^0) = 0.410(2)$ ps and $\tau(D^+) = 1.040(7)$ ps, the results are collected in Table 6. Compared with other theoretical and Lattice [63] predictions, our results are smaller, which is more consistent with the BESIII [16–18] experiment within errors.

3.2.2 Polarization observations

Due to the current experimental conditions, it is difficult to measure the q^2 dependence of polarization observation. However, it is very important to study the q^2 dependence of these physical observables. On the one hand, it can facilitate the comparison among theories; on the other hand, it also provides references for experimental research on q^2 dependence and more details for exploring new physics.

We firstly show final state polarization $P_{L,T}^\ell$ and $F_{L,T}^\ell$ in the Fig. 4.

- For the left panel, the final lepton polarization for the $D \rightarrow V(\rho, \omega, K^*)\ell^+\nu_\ell$ are shown and calculated by Eq. (2.8). All $P_{L,T}^\ell$ polarizations exhibit similar behavior. In the large q^2 region, all polarizations are almost unchanged, except that P_T^μ rise slowly with the increase of q^2 , i.e. $P_L^\ell \approx 1$, $P_T^e \approx 0$ and $P_T^\mu \lesssim 0$. In the low q^2 region, all $P_{L,T}^\ell$ polarities are singular due to the δ_ℓ factor, which are clearly shown in the corresponding small graph with the logarithmic axis. We find that $P_L^{e(\mu)}$ are approximately equal to -0.4 at $q_{\min}^2 = m_{e(\mu)}^2$. As q^2 increases, $P_L^{e(\mu)}$ then rapidly increases to near 1 and final remains stable. For transverse component, $P_T^{e,\mu}(q_{\min}^2 = m_{e(\mu)}^2) \approx -0.8$. As q^2 increases, P_T^μ

Table 6. Branching fractions for semileptonic D decays i.e. $D \rightarrow V(\rho, \omega, K^*)\ell^+\nu_\ell$ (in unit: 10^{-3} for ρ and ω mesons; 10^{-2} for K^* meson), where the uncertainties are the squared average of all the input parameters. The current theoretical and experimental results in references are also listed as a comparison.

	$D^0 \rightarrow \rho^- e^+ \nu_e$	$D^0 \rightarrow \rho^- \mu^+ \nu_\mu$	$D^+ \rightarrow \rho^0 e^+ \nu_e$	$D^+ \rightarrow \rho^0 \mu^+ \nu_\mu$	$D^+ \rightarrow \omega e^+ \nu_e$
This Work	$1.440^{+0.277}_{-0.250}$	$1.432^{+0.274}_{-0.248}$	$1.827^{+0.351}_{-0.317}$	$1.816^{+0.348}_{-0.314}$	$1.740^{+0.482}_{-0.399}$
CCQM[60]	1.62	1.55	2.09	2.01	1.85
LFQM[67]	-	-	-	-	2.1(2)
χ UA [68]	1.97	1.84	2.54	2.37	2.46
LCSR[69]	$1.81^{+0.18}_{-0.13}$	$1.73^{+0.17}_{-0.13}$	$2.29^{+0.23}_{-0.16}$	$2.20^{+0.21}_{-0.16}$	$1.93^{+0.20}_{-0.14}$
Lattice[63]	-	-	2.23(70)	2.13(64)	-
BESIII[16–18]	1.445(70)	-	1.860(93)	-	1.63(14)
CLEO[24–26]	1.77(16)	-	$2.17(12)(^{+0.12}_{-0.22})$	-	1.82(19)
PDG[59]	-	-	-	2.4(4)	-
	$D^+ \rightarrow \omega \mu^+ \nu_\mu$	$D^0 \rightarrow K^{*-} e^+ \nu_e$	$D^0 \rightarrow K^{*-} \mu^+ \nu_\mu$	$D^+ \rightarrow \bar{K}^{*0} e^+ \nu_e$	$D^+ \rightarrow \bar{K}^{*0} \mu^+ \nu_\mu$
This Work	$1.728^{+0.479}_{-0.397}$	$2.082^{+0.334}_{-0.314}$	$2.066^{+0.330}_{-0.310}$	$5.282^{+0.847}_{-0.796}$	$5.242^{+0.838}_{-0.787}$
CCQM[60]	1.78	2.96	2.80	7.61	7.21
LFQM[67]	2.0(2)	-	-	7.5(7)	7.0(7)
χ UA [68]	2.29	2.15	1.98	5.56	5.12
LCSR[69]	$1.85^{+0.19}_{-0.13}$	2.12(9)	$2.01^{+0.09}_{-0.08}$	$5.37^{+0.24}_{-0.23}$	$5.10^{+0.23}_{-0.21}$
Lattice[63]	-	-	-	6.26(184)	5.95(167)
BESIII[16–18]	1.77(29)	2.033(66)	-	-	-
CLEO[24–26]	-	2.16(17)	-	-	5.27 ± 0.16
PDG[59]	-	-	-	5.4(1)	-

rapidly increases to near 0 and then remains stable, while P_T^e increase rapidly and then slowly.

- For the right panel, the longitudinal $F_L^\ell(q^2)$ and transverse $F_T^\ell(q^2)$ polarization fractions of the vector meson are shown and calculated by using the Eq. (2.8), which indicate the three kinds of vector ρ, ω, K^* mesons have the similar behavior for both $F_L^\ell(q^2)$ and $F_T^\ell(q^2)$. At all the allowed physical region, we have $F_L^\ell(q^2) + F_T^\ell(q^2) = 1$. For the large recoil point $q^2 = 0 \text{ GeV}^2$, we find $F_L^\ell(0) = 1$ and $F_T^\ell(0) = 0$. As the q^2 increases, $F_L^\ell(q^2)$ monotonically decreases, and the $F_T^\ell(q^2)$ reverses. In addition, $F_L^\ell(q^2)$ is dominant in the small q^2 region, while $F_T^\ell(q^2)$ is dominant in the large q^2 region. The dominant alternate

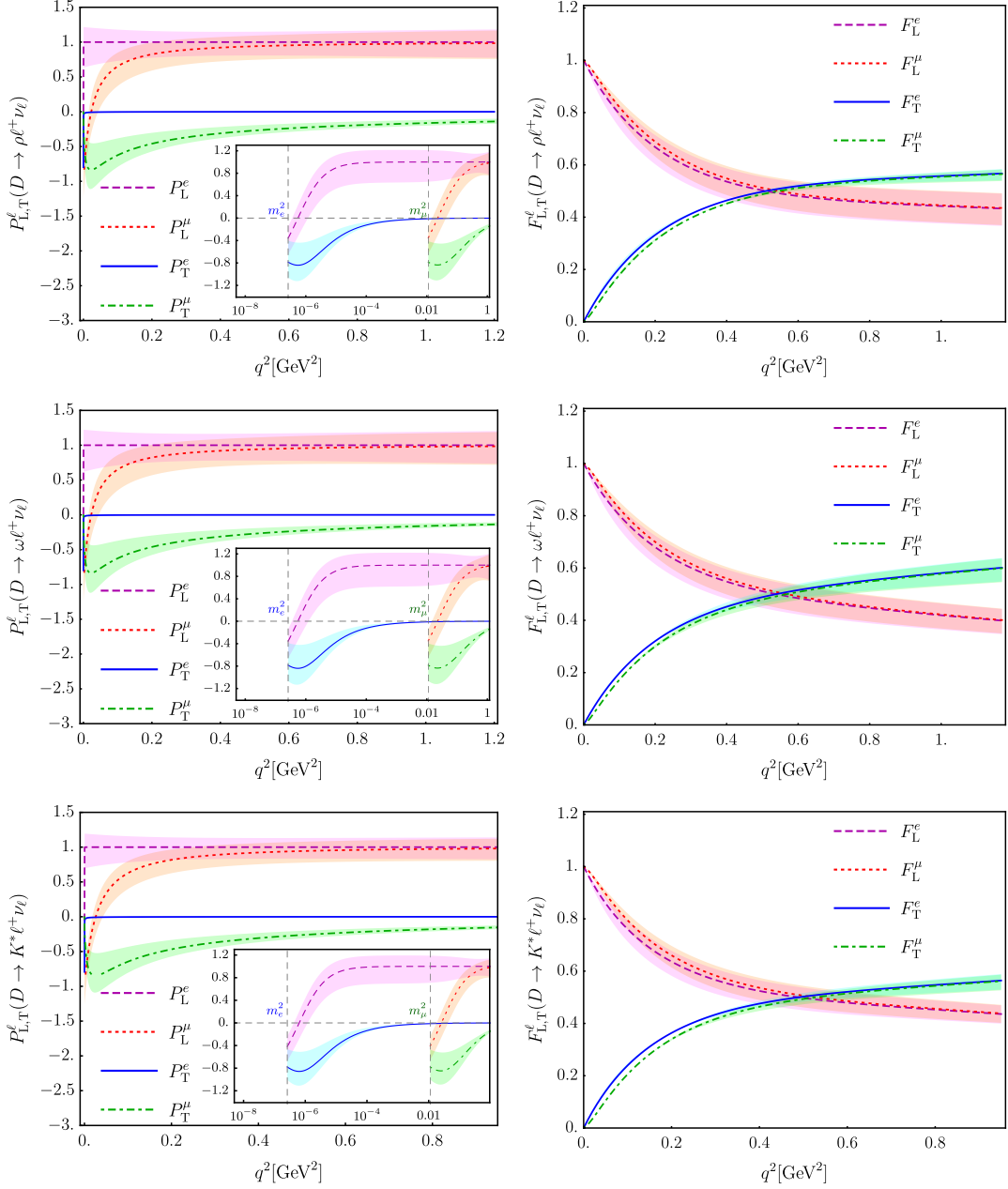


Figure 4. The final state polarization $P_{L,T}^\ell$ and $F_{L,T}^\ell$ as a function of q^2 for the $D \rightarrow V \ell^+ \nu_\ell$. Here P and F represent charged lepton and vector meson in the final state, which corresponds to the left and right panels respectively; T and L are longitudinal and transverse fractions; V stands for the ρ, ω, K^* mesons corresponding to upper, medial and bottom part respectively. In which the dashed-, dotted-, dot-dashed- and solid-line represent the corresponding central values, and the shaded band is the corresponding errors from HFFs.

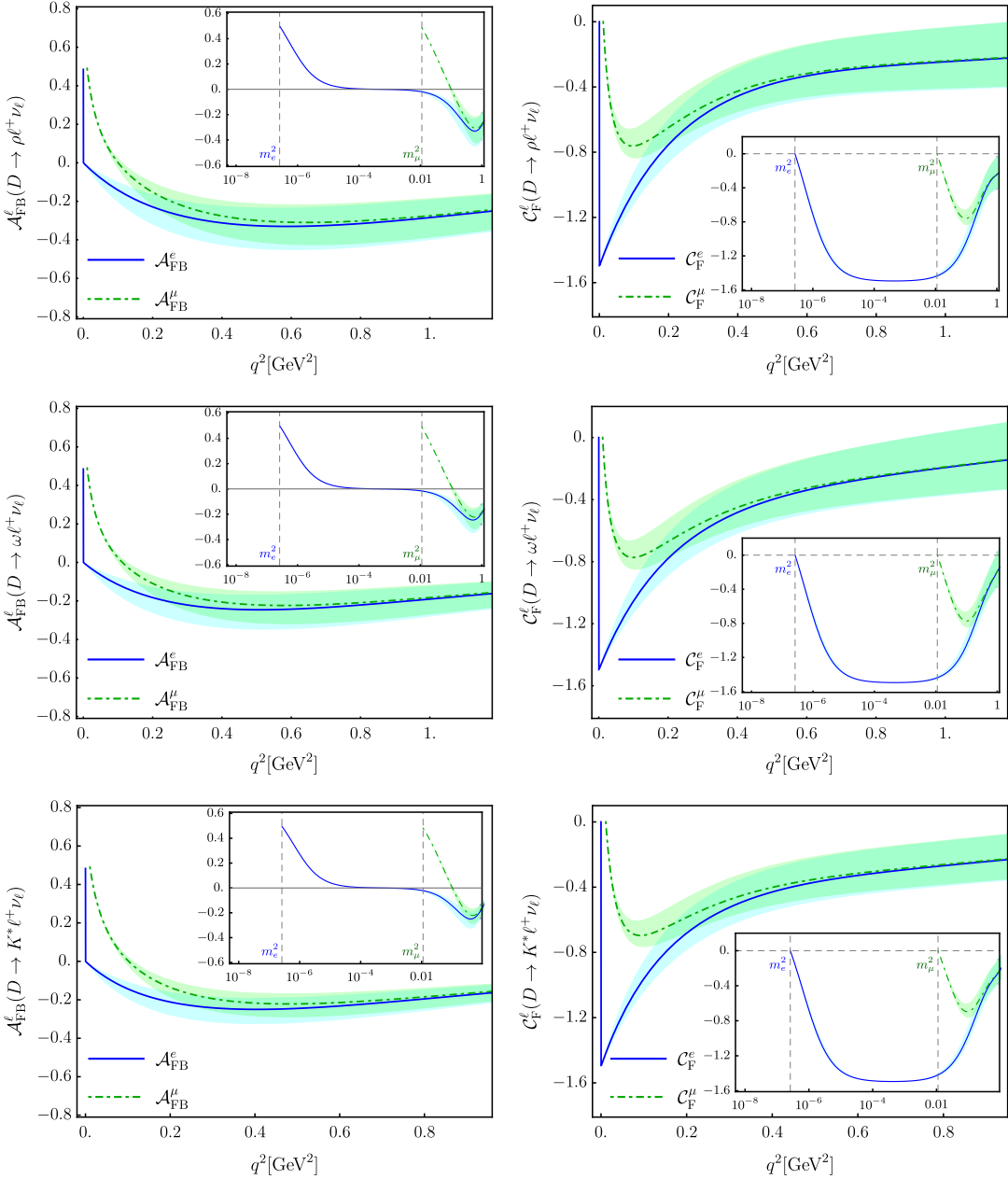


Figure 5. Forward-backward asymmetry $\mathcal{A}_{\text{FB}}^{\ell}(q^2)$ and the lepton-side $\mathcal{C}_{\text{F}}^{\ell}(q^2)$ convexity parameter as a function of q^2 for the $D \rightarrow V(\rho, \omega, K^*)\ell^+\nu_{\ell}$. The lines are their central values and the shaded bands are their errors. The meaning of corresponding representations can refer to Fig. 4.

point is located near the midpoint of the whole physical region. At the alternate point q_{mix}^2 , we find $F_{\text{L}}^{\ell} = F_{\text{T}}^{\ell} = 0.5$ due to the relation $F_{\text{L}}^{\ell}(q^2) + F_{\text{T}}^{\ell}(q^2) = 1$.

Table 7. The mean values for longitudinal and transverse polarizations fraction of final lepton and vector mesons, forward-backward asymmetry and the lepton-side convexity parameter for positron and muon modes, where the uncertainties are the squared average of all the input parameters.

$D \rightarrow \rho \ell^+ \nu_\ell$		$D \rightarrow \omega \ell^+ \nu_\ell$		$D \rightarrow K^* \ell^+ \nu_\ell$	
This Work	CCQM [60]	This Work	CCQM [60]	This Work	CCQM [60]
$\langle P_L^e \rangle$	$+1.000^{+0.168}_{-0.209}$	+1.00	$+1.000^{+0.188}_{-0.244}$	+1.00	$+1.000^{+0.136}_{-0.170}$
$\langle P_L^\mu \rangle$	$+0.968^{+0.170}_{-0.211}$	+0.92	$+0.969^{+0.190}_{-0.245}$	0.92	$+0.958^{+0.138}_{-0.171}$
$\langle P_T^e \rangle \times 10^2$	$-0.093^{+0.026}_{-0.114}$	-0.09	$-0.092^{+0.024}_{-0.018}$	-0.09	$-0.106^{+0.023}_{-0.019}$
$\langle P_T^\mu \rangle$	$-0.189^{+0.042}_{-0.053}$	-0.13	$-0.186^{+0.048}_{-0.037}$	-0.12	$-0.213^{+0.046}_{-0.038}$
$\langle F_L^e \rangle$	$+0.457^{+0.055}_{-0.067}$	+0.53	$+0.441^{+0.045}_{-0.057}$	+0.52	$+0.472^{+0.036}_{-0.042}$
$\langle F_L^\mu \rangle$	$+0.461^{+0.053}_{-0.065}$	+0.51	$+0.445^{+0.044}_{-0.055}$	+0.50	$+0.478^{+0.035}_{-0.041}$
$\langle \mathcal{A}_{FB}^e \rangle$	$-0.293^{+0.094}_{-0.117}$	-0.21	$-0.203^{+0.071}_{-0.094}$	-0.21	$-0.208^{+0.052}_{-0.066}$
$\langle \mathcal{A}_{FB}^\mu \rangle$	$-0.279^{+0.091}_{-0.113}$	-0.24	$-0.191^{+0.068}_{-0.090}$	-0.24	$-0.192^{+0.049}_{-0.062}$
$\langle \mathcal{C}_F^e \rangle$	$-0.278^{+0.165}_{-0.205}$	-0.44	$-0.242^{+0.173}_{-0.222}$	-0.43	$-0.312^{+0.123}_{-0.151}$
$\langle \mathcal{C}_F^\mu \rangle$	$-0.268^{+0.162}_{-0.199}$	-0.36	$-0.233^{+0.169}_{-0.216}$	-0.35	$-0.297^{+0.119}_{-0.146}$

We then plot the forward-backward asymmetry \mathcal{A}_{FB}^ℓ and the lepton-side $\mathcal{C}_F^\ell(q^2)$ convexity parameter in Fig. 5.

- The left panel of Fig. 5 show the change of forward-backward asymmetry \mathcal{A}_{FB}^ℓ from $q_{\min}^2 = m_\ell^2$ to $q_{\max}^2 = (m_D - m_V)^2$. All \mathcal{A}_{FB}^ℓ are, first down from positive value to 0 rapidly, then slowly down to the minimum value, and finally almost horizontal slowly up. $\mathcal{A}_{FB}^{e(\mu)} = 0$ is around $q^2 = 0.1$ GeV 2 ($q^2 = 10^{-4}$ GeV 2), and all $\mathcal{A}_{FB,\max}^\ell \approx 0.5$ are show in the small figure at $q^2 = m_e^2$ ($q^2 = m_\mu^2$). All of these phenomena can be derived from its analytic expression Eq. (2.9). Therefore, one shall be especially careful when dealing with \mathcal{A}_{FB}^ℓ in the small q^2 region, while it will be easier to study in the large q^2 region due to the relatively stable value of the \mathcal{A}_{FB}^ℓ .
- For the right panel of Fig. 5, we find that $\mathcal{C}_F^\ell(q^2) \leq 0$, $\mathcal{C}_F^\ell(q_{\min}^2 = m_{e,\mu}^2) = 0$. All the $\mathcal{C}_F^\ell(q^2)$ decrease sharply and then increase, and there is a singularity around low q^2 , which are exhibited in the small graph with the logarithmic axis.

The mean values of those polarization observations for the three $D \rightarrow V$ semileptonic decay channels are calculated by applying Eq. (2.11) and listed in Table 7. Our predictions are the same with the CCQM results within errors.

4 Summary

In this paper, $D \rightarrow V(\omega, \rho, K^*)$ HFFs $\mathcal{D}_{V,\sigma}$ with $\sigma = 0, 1, 2, t$ have been studied by applying the LCSR and taking into account the LCDAs up to twist-4. The resultant LCSRs for the HFFs are arranged according to the twist structure of the final vector meson LCDAs. Those HFFs are extrapolated to the whole physics q^2 -region $m_\ell^2 \leq q^2 \leq (m_D - m_V)^2$, and then we use it to investigate the physical observables for the $D \rightarrow V(\rho, \omega, K^*)\ell^+\nu_\ell$ semileptonic decays.

The depression-effect for the transversal HFFs and its errors increase as q^2 decrease due to its q^2 coefficient, especially for $\mathcal{D}_{V,1,2}(0) = 0(\pm 0)$ with $V = \rho, \omega, K^*$. This depression-effect will also be reflected in the different transverse decay width through transversal HFFs, which can be clearly seen from the Fig. 3, we also have $1/|V_{cq}|^2 \times d\Gamma_V^T(0) = 0(\pm 0)$ with $V = \rho, \omega, K^*$ mesons. However, the depression-effect feature for the longitudinal part will disappear as q^2 coefficient missing. Thus, in the small q^2 region, the transverse differential decay width dominates, while in the large q^2 region, the longitudinal differential decay width dominates, and the dominant alternate point is near the midpoint of the whole physically feasible region. In addition, the decay width (transverse, longitudinal and total decay width) decreases with the increase of the mass of the final state of the meson, and the absolute change number of the transverse and longitudinal are almost the same, which can be seen from the Table 4. With the help of lifetime $\tau(D^0)$ and $\tau(D^+)$, we calculate the branching ratio and list it in Table 6. Our predictions are lower compared to other theories, but it fits well with BES-III.

We also investigate in detail the q^2 dependence behavior of polarization observations for $D \rightarrow V(\rho, \omega, K^*)\ell^+\nu_\ell$ semileptonic decays with $\ell = e, \mu$, which has a similar shape for different final meson and same final lepton. In the small q^2 region, all those polarization observations have a singularity due to the δ_ℓ factor, which are shown in the small graph with the logarithmic axis, expect for $F_{L,T}^\ell$. With the increase of q^2 , all polarization values tend to be more stable, thus the polarization dependence on q^2 is reducing. Note that F_L^ℓ and F_T^ℓ dominated the small q^2 region and the large q^2 region respectively, and the alternating points of the dominant region are around the center of the corresponding all physical regions, which roughly equates to the positions of the dominant alternating points of the transverse and longitudinal differential decay width. We also calculate the corresponding average values and list it in Table 7, which are in good agreement with CCQM within the errors.

Acknowledgments

We are grateful to Prof. Xing-Gang Wu and Tao Zhong for many helpful discussions and suggestions. This work was supported in part by the National Natural Science Foundation of China under Grant No.11765007, 11947302, the Project of Guizhou Provincial Department of Science and Technology under Grant No.KY[2017]1089 and No.KY[2019]1171, the China Postdoctoral Science Foundation under Grant No.2019TQ0329.

Table 8. The moments and couplings of vector meson twist-2,3,4 LCDA, the corresponding scale are $\mu^2 = m_D^2 - m_c^2 \approx 1\text{GeV}^2$.

	ρ	ω	K^*
a_1^{\parallel}	0	0	0.19(5)
a_2^{\parallel}	0.18(10)	0.18(10)	0.06(6)
a_1^{\perp}	0	0	0.20(5)
a_2^{\perp}	0.20(10)	0.18(10)	0.04(4)
δ_+	0	0	0.24
δ_-	0	0	-0.24
$\tilde{\delta}_+$	0	0	0.16
$\tilde{\delta}_-$	0	0	-0.16

Appendix

In order to get the accurate HFFs results within LCSR approach for the semileptonic decay processes $D \rightarrow V(\rho, \omega, K^*)\ell^+\nu_\ell$ and make a comparison with other theoretical and experimental results, we take the twist-2,3,4 LCDAs given by P. Ball and V. M. Braun [62] used by many theoretical predictions. The twist-3 LCDAs of the two-particle distribution has the following form,

$$\psi_{3;V}^{\perp}(u) = 6u\bar{u} \left[1 + a_1^{\parallel}\xi + \left\{ \frac{1}{4}a_2^{\parallel} + \frac{5}{3}\zeta_3 \left(1 - \frac{3}{16}\omega_3^A + \frac{9}{16}\omega_3^V \right) \right\} (5\xi^2 - 1) \right] + 6\tilde{\delta}_+ (3u\bar{u} + \bar{u}\ln\bar{u} + u\ln u) + 6\tilde{\delta}_- (\bar{u}\ln\bar{u} - u\ln u), \quad (4.1)$$

$$\phi_{3;V}^{\perp}(u) = \frac{3}{4}(1 + \xi^2) + a_1^{\parallel}\frac{3}{2}\xi^3 + \left(\frac{3}{7}a_2^{\parallel} + 5\zeta_3 \right) (3\xi^2 - 1) + \left[\frac{9}{112}a_2^{\parallel} + \frac{15}{64}\zeta_3 (3\omega_3^V - \omega_3^A) \right] \times (3 - 30\xi^2 + 35\xi^4) + \frac{3}{2}\tilde{\delta}_+ (2 + \ln u + \ln\bar{u}) + \frac{3}{2}\tilde{\delta}_- (2\xi + \ln\bar{u} - \ln u), \quad (4.2)$$

$$\psi_{3;V}^{\parallel}(u) = 6u\bar{u} \left[1 + a_1^{\perp}\xi + \left(\frac{1}{4}a_2^{\perp} + \frac{5}{8}\zeta_3\omega_3^T \right) (5\xi^2 - 1) \right] + 3\delta_+ (3u\bar{u} + \bar{u}\ln\bar{u} + u\ln u) + 3\delta_- (\bar{u}\ln\bar{u} - u\ln u), \quad (4.3)$$

$$\phi_{3;V}^{\parallel}(u) = 3\xi^2 + \frac{3}{2}a_1^{\perp}\xi(3\xi^2 - 1) + \frac{3}{2}a_2^{\perp}\xi^2(5\xi^2 - 3) + \frac{15}{16}\zeta_3\omega_3^T(3 - 30\xi^2 + 35\xi^4) + \frac{3}{2}\delta_+ \times \left(1 + \xi\ln\frac{\bar{u}}{u} \right) + \frac{3}{2}\delta_- \xi(2 + \ln u + \ln\bar{u}). \quad (4.4)$$

And the twist-4 LCDA for the two-particle distributions can be written as

$$\psi_{4;V}^\perp(u) = 6u(1-u) + 5 \left[\zeta_4^T + \tilde{\zeta}_4^T \right] (1-3\xi^2), \quad (4.5)$$

$$\phi_{4;V}^\perp(u) = 30u^2(1-u)^2 \left[\frac{2}{5} + \frac{4}{3}\zeta_4^T - \frac{8}{3}\tilde{\zeta}_4^T \right], \quad (4.6)$$

$$\phi_{4;V}^\parallel(u) = \left[\frac{4}{5} + \frac{20}{9}\zeta_4 + \frac{8}{9}\zeta_3 \right] 30u^2\bar{u}^2, \quad (4.7)$$

$$\psi_{4;V}^\parallel(u) = 6u\bar{u} + \left[\frac{10}{3}\zeta_4 - \frac{20}{3}\zeta_3 \right] (1-3\xi^2), \quad (4.8)$$

$$C_V(u) = \left[\frac{3}{2} + \frac{10}{3}\zeta_4 + \frac{10}{3}\zeta_3 \right] u^2\bar{u}^2, \quad (4.9)$$

The values of the moments and coupling constants of the vector meson twist-2,3,4 LCDAs are listed in Table 8. At the scale $\mu^2 = m_D^2 - m_c^2 \approx 1\text{GeV}^2$, the couplings for twist-3 and twist-4 LCDAs are

$$\zeta_3 = 0.032, \quad \omega_3^A = -2.1, \quad \omega_3^V = 3.8, \quad \omega_3^T = 7.0, \quad \zeta_4 = 0.15, \quad \zeta_4^T = 0.10, \quad \tilde{\zeta}_4^T = -0.10. \quad (4.10)$$

References

- [1] J. Charles *et al.* [CKMfitter Group], CP violation and the CKM matrix: Assessing the impact of the asymmetric B factories, *Eur. Phys. J. C* **41** (2005) 1.
- [2] A. Poluektov *et al.* [Belle Collaboration], Evidence for direct CP violation in the decay $B^\pm \rightarrow D^{(*)}K^\pm, D \rightarrow K_s^0\pi + \pi^-$ and measurement of the CKM phase ϕ_3 , *Phys. Rev. D* **81** (2010) 112002.
- [3] M. Bona, A. Contu, G. Fedi and M. J. Morello, CKM matrix and CP violation in charm and beauty, *PoS PP@LHC2016* (2016) 009.
- [4] K. Abe *et al.* [T2K Collaboration], Search for CP Violation in Neutrino and Antineutrino Oscillations by the T2K Experiment with 2.2×10^{21} Protons on Target, *Phys. Rev. Lett.* **121** (2018) 171802.
- [5] R. Aaij *et al.* [LHCb Collaboration], Observation of CP Violation in Charm Decays, *Phys. Rev. Lett.* **122**, 211803 (2019).
- [6] S. Funatsu, H. Hatanaka, Y. Hosotani, Y. Orikasa and N. Yamatsu, CKM matrix and FCNC suppression in $SO(5) \times U(1) \times SU(3)$ gauge-Higgs unification, *Phys. Rev. D* **101** (2020) 055016.
- [7] P. K. Resmi *et al.* [Belle Collaboration], First measurement of the CKM angle ϕ_3 with $B^\pm \rightarrow D(K_S^0\pi^+\pi^-\pi^0)K^\pm$ decays, *JHEP* **1910** (2019) 178.

[8] B. Belfatto, R. Beradze and Z. Berezhiani, The CKM unitarity problem: A trace of new physics at the TeV scale?, *Eur. Phys. J. C* **80** (2020) 149.

[9] J. Drobna, S. Fajfer and J. F. Kamenik, Signatures of NP models in top FCNC decay $t \rightarrow c(u)\ell^+\ell^-$, *JHEP* **0903** (2009) 077.

[10] F. J. Botella, G. C. Branco, A. Carmona, M. Nebot, L. Pedro and M. N. Rebelo, Physical Constraints on a Class of Two-Higgs Doublet Models with FCNC at tree level, *JHEP* **1407** (2014) 078.

[11] C. S. Kim, Y. W. Yoon and X. B. Yuan, Exploring top quark FCNC within 2HDM type III in association with flavor physics, *JHEP* **1512** (2015) 038.

[12] D. Melikhov, A. Kozachuk and N. Nikitin, Rare FCNC radiative leptonic $B_{s,d} \rightarrow \gamma\ell^+\ell^-$ decays in the SM, *PoS Confinement* **2018** (2019) 274.

[13] K. Y. Oyulmaz, A. Senol, H. Denizli and O. Cakir, Top quark anomalous FCNC production via tqg couplings at FCC-hh, *Phys. Rev. D* **99** (2019) 115023.

[14] M. Ablikim *et al.* [BESIII Collaboration], Observation of the Singly Cabibbo-Suppressed Decay $D^+ \rightarrow \omega\pi^+$ and Evidence for $D^0 \rightarrow \omega\pi^0$, *Phys. Rev. Lett.* **116** (2016) 082001.

[15] M. Ablikim *et al.* [BESIII Collaboration], Measurement of the absolute branching fraction of $D^+ \rightarrow \bar{K}^0 e^+ \nu_e$ via $\bar{K}^0 \rightarrow \pi^0 \pi^0$, *Chin. Phys. C* **40** (2016) 113001.

[16] M. Ablikim *et al.* (BESIII Collaboration), Measurement of the form factors in the decay $D^+ \rightarrow \omega e^+ \nu_e$ and search for the decay $D^+ \rightarrow \phi e^+ \nu_e$, *Phys. Rev. D* **92**, 071101 (2015).

[17] M. Ablikim *et al.* (BESIII Collaboration), First Observation of $D^+ \rightarrow f_0(500)e^+ \nu_e$ and Improved Measurements of $D \rightarrow \rho e^+ \nu_e$, *Phys. Rev. Lett.* **122**, 062001 (2019).

[18] M. Ablikim *et al.* (BESIII Collaboration), Study of the decay $D^0 \rightarrow \bar{K}^0 \pi^- e^+ \nu_e$, *Phys. Rev. D* **99**, 011103 (2019).

[19] K. Liu [BESIII Collaboration], Semileptonic and leptonic D decays at BESIII, *PoS LeptonPhoton* **2019** (2019) 046.

[20] M. Ablikim *et al.* [BESIII Collaboration], Measurement of branching fractions for D meson decaying into ϕ meson and a pseudoscalar meson, *Phys. Lett. B* **798** (2019) 135017.

[21] P. Naik *et al.* [CLEO Collaboration], Measurement of the Pseudoscalar Decay Constant f_{D_s} Using $D_s^+ \rightarrow \tau^+ \nu, \tau^+ \rightarrow \rho^+ \bar{\nu}$ Decays, *Phys. Rev. D* **80** (2009) 112004.

[22] L. Martin *et al.* [CLEO Collaboration], Search for the decay $D_s^+ \rightarrow \omega e^+ \nu$, *Phys. Rev. D* **84**, 012005 (2011).

[23] P. U. E. Onyisi *et al.* [CLEO Collaboration], Improved Measurement of Absolute Hadronic Branching Fractions of the D_s^+ Meson, *Phys. Rev. D* **88** (2013) 032009.

[24] T. E. Coan *et al.* (CLEO Collaboration), Absolute branching fraction measurements of exclusive D0 semileptonic decays, *Phys. Rev. Lett.* **95**, 181802 (2005).

[25] R. A. Briere *et al.* (CLEO Collaboration), Analysis of $D^+ \rightarrow K^- \pi^+ e^+ \nu_e$ and $D^+ \rightarrow K^- \pi^+ \mu^+ \nu_\mu$ Semileptonic Decays, *Phys. Rev. D* **81**, 112001 (2010).

[26] S. Dobbs *et al.* (CLEO Collaboration), First Measurement of the Form Factors in the Decays $D^0 \rightarrow \rho^- e^+ \nu_e$ and $D^+ \rightarrow \rho^0 e^+ \nu_e$, *Phys. Rev. Lett.* **110**, 131802 (2013).

[27] [BESIII Collaboration], Observation of the semi-muonic decay $D^+ \rightarrow \omega \mu^+ \nu_\mu$, arXiv:2002.10578 [hep-ex].

[28] Y. Grossman and D. Pirjol, Extracting and using photon polarization information in radiative B decays, JHEP **0006**, 029 (2000).

[29] M. Gronau, Y. Grossman, D. Pirjol and A. Ryd, Measuring the photon polarization in $B \rightarrow K\pi\pi\gamma$, Phys. Rev. Lett. **88** (2002) 051802.

[30] F. Kruger and J. Matias, Probing new physics via the transverse amplitudes of $B^0 \rightarrow K^{*0}(\rightarrow K^-\pi^+)\ell^+\ell^-$ at large recoil, Phys. Rev. D **71** (2005) 094009.

[31] E. Kou, A. Le Yaouanc and A. Tayduganov, Determining the photon polarization of the $b \rightarrow s\gamma$ using the $B \rightarrow K_1(1270)\gamma \rightarrow (K\pi\pi)\gamma$ decay, Phys. Rev. D **83** (2011) 094007.

[32] S. Wehle, Angular Analysis of $B \rightarrow K^*\ell\ell$ and Search for $B^+ \rightarrow K^+\tau\tau$ at the Belle Experiment, doi:10.3204/PUBDB-2016-03770.

[33] W. Cheng, X. G. Wu and H. B. Fu, Reconsideration of the $B \rightarrow K^*$ transition form factors within the QCD light-cone sum rules, Phys. Rev. D **95** (2017) 094023.

[34] H. B. Fu, X. G. Wu, W. Cheng, T. Zhong and Z. Sun, Asymmetries of the $B \rightarrow K^*\mu^+\mu^-$ decay and the search of new physics beyond the standard model, Phys. Rev. D **97** (2018) 055037.

[35] R. Y. Zhou, L. Guo, H. B. Fu, W. Cheng and X. G. Wu, The $B \rightarrow \pi\ell\nu_\ell$ semileptonic decay within the LCSR approach under heavy quark effective field theory,” Chin. Phys. C **44** (2020) 013101.

[36] W. Wang, F. S. Yu and Z. X. Zhao, Model-Independent Determination of Photon Helicity in Radiative $B \rightarrow K_1\gamma$ Decays, arXiv:1909.13083 [hep-ph].

[37] L. M. Garca Martn, B. Jashal, F. Martnez Vidal, A. Oyanguren, S. Roy, R. Sain and R. Sinha, Radiative b -baryon decays to measure the photon and b -baryon polarization, Eur. Phys. J. C **79** (2019) 634.

[38] V. M. Braun, Light cone sum rules, hep-ph/9801222.

[39] T. Huang and Z. H. Li, $B \rightarrow K^*\gamma$ in the light cone QCD sum rule, Phys. Rev. D **57**, 1993 (1998).

[40] T. Huang, Z. H. Li and X. Y. Wu, Improved approach to the heavy to light form-factors in the light cone QCD sum rules, Phys. Rev. D **63**, 094001 (2001).

[41] X. G. Wu, T. Huang and Z. Y. Fang, $SU_f(3)$ symmetry breaking effects of the $B \rightarrow K$ transition form-factor in the QCD light-cone sum rules, Phys. Rev. D **77**, 074001 (2008).

[42] S. Momeni, R. Khosravi and F. Falahati, Flavor changing neutral current transition of $B \rightarrow a_1$ with light-cone sum rules, Phys. Rev. D **95** (2017) 016009.

[43] Y. M. Wang, Y. B. Wei, Y. L. Shen and C. D. L, Perturbative corrections to $B \rightarrow D$ form factors in QCD, JHEP **1706** (2017) 062.

[44] X. D. Cheng, H. B. Li, B. Wei, Y. G. Xu and M. Z. Yang, Study of $D \rightarrow a_0(980)e^+\nu_e$ decay in the light-cone sum rules approach, Phys. Rev. D **96** (2017) 033002.

[45] H. B. Fu, L. Zeng, R. L. W. Cheng and X. G. Wu, The $D \rightarrow \rho$ semileptonic and radiative decays within the light-cone sum rules, *Eur. Phys. J. C* **80** (2020) 194.

[46] J. Gao, C. D. L, Y. L. Shen, Y. M. Wang and Y. B. Wei, Precision calculations of $B \rightarrow V$ form factors in QCD, arXiv:1907.11092 [hep-ph].

[47] S. Momeni and R. Khosravi, Semileptonic $D_{(s)} \rightarrow A\ell^+\nu$ and nonleptonic $D \rightarrow K_1(1270, 1400)\pi$ decays in LCSR, *J. Phys. G* **46** (2019) 105006.

[48] I. I. Balitsky, V. M. Braun and A. V. Kolesnichenko, Radiative Decay $\sigma^+ \rightarrow p\gamma$ in Quantum Chromodynamics, *Nucl. Phys. B* **312**, 509 (1989).

[49] V. L. Chernyak and I. R. Zhitnitsky, B meson exclusive decays into baryons, *Nucl. Phys. B* **345**, 137 (1990).

[50] V. M. Belyaev, A. Khodjamirian and R. Rückl, QCD calculation of the $B \rightarrow \pi, K$ form-factors, *Z. Phys. C* **60**, 349 (1993).

[51] P. Ball and V. M. Braun, Use and misuse of QCD sum rules in heavy to light transitions: The Decay $B \rightarrow \rho e\nu$ reexamined, *Phys. Rev. D* **55**, 5561 (1997).

[52] P. Ball and R. Zwicky, $B_{(ds)} \rightarrow \rho, \omega, K^*, \phi$ decay form-factors from light-cone sum rules revisited, *Phys. Rev. D* **71**, 014029 (2005).

[53] S. Fajfer and J. F. Kamenik, Charm meson resonances and $D \rightarrow V$ semileptonic form-factors, *Phys. Rev. D* **72**, 034029 (2005).

[54] W. Wang and Y. L. Shen, $D_s \rightarrow K, K^*, \phi$ form factors in the Covariant Light-Front Approach and Exclusive D_s Decays, *Phys. Rev. D* **78**, 054002 (2008).

[55] W. Cheng, X. G. Wu, R. Y. Zhou and H. B. Fu, The $B \rightarrow \rho$ helicity form factors within the QCD light-cone sum rules, *Phys. Rev. D* **98** (2018) 096013.

[56] A. Bharucha, T. Feldmann and M. Wick, Theoretical and Phenomenological Constraints on Form Factors for Radiative and Semi-Leptonic B -Meson Decays, *JHEP* **1009** (2010) 090.

[57] H. B. Fu, W. Cheng, R. Y. Zhou and L. Zeng, $D \rightarrow P(\pi, K)$ helicity form factors within LCSR, arXiv:2002.11279 [hep-ph].

[58] D. Leljak, B. Melic and M. Patra, On lepton flavour universality in semileptonic $B_c \rightarrow \eta_c, J/\psi$ decays, *JHEP* **1905**, 094 (2019).

[59] M. Tanabashi *et al.* [Particle Data Group], Review of Particle Physics, *Phys. Rev. D* **98**, 030001 (2018).

[60] M. A. Ivanov, J. G. Körner, J. N. Pandya, P. Santorelli, N. R. Soni and C. T. Tran, Exclusive semileptonic decays of D and D_s mesons in the covariant confining quark model, *Front. Phys. (Beijing)* **14**, 64401 (2019).

[61] H. B. Fu, X. G. Wu, H. Y. Han and Y. Ma, $B \rightarrow \rho$ transition form factors and the ρ meson transverse leading-twist distribution amplitude, *J. Phys. G* **42** (2015) 055002.

[62] P. Ball and V. M. Braun, Exclusive semileptonic and rare B meson decays in QCD, *Phys. Rev. D* **58**, 094016 (1998).

[63] D. Melikhov and B. Stech, Weak form-factors for heavy meson decays: An Update, *Phys. Rev. D* **62**, 014006 (2000).

- [64] W. Y. Wang, Y. L. Wu, and M. Zhong, Heavy to light meson exclusive semileptonic decays in effective field theory of heavy quarks, *Phys. Rev. D* **67**, 014024 (2003).
- [65] P. Ball, V. M. Braun, and H. G. Dosch, Form-factors of semileptonic D decays from QCD sum rules, *Phys. Rev. D* **44**, 3567 (1991).
- [66] C. R. Allton *et al.* (APE Collaboration), Lattice calculation of D and B meson semileptonic decays using the Clover action at $\beta = 6.0$ on APE, *Phys. Lett. B* **345**, 513 (1995).
- [67] H. Y. Cheng and X. W. Kang, Branching fractions of semileptonic D and D_s decays from the covariant light-front quark model, *Eur. Phys. J. C* **77**, 587 (2017).
- [68] T. Sekihara and E. Oset, Investigating the nature of light scalar mesons with semileptonic decays of D mesons, *Phys. Rev. D* **92**, 054038 (2015).
- [69] Y. L. Wu, M. Zhong, and Y. B. Zuo, $B_{(s)}, D_{(s)} \rightarrow \pi, K, \eta, \rho, K^*, \omega, \phi$ Transition Form Factors and Decay Rates with Extraction of the CKM parameters $|V_{ub}|, |V_{cs}|, |V_{cd}|$, *Int. J. Mod. Phys. A* **21**, 6125 (2006).